Experimental Thermal and Fluid Science 124 (2021) 110349

Contents lists available at ScienceDirect

Experimental Thermal and Fluid Science

journal homepage: www.elsevier.com/locate/etfs

Experimental investigation of the characteristics of the transition from spherical cap bubble to slug flow in a vertical pipe

M. Abdulkadir [a,*], B. Ugwoke [b,d], L.A. Abdulkareem [c], D. Zhao [b,d], V. Hernandez-Perez [e]

[a] Chemical Engineering Department, Federal University of Technology, Minna, Niger State, Nigeria
[b] Energy Department, Politecnico di Torino, Italy
[c] Petroleum Engineering Department, College of Engineering, University of Zakho
[d] School of Engineering, London South Bank University, London, United Kingdom
[e] Department of Mechanical Engineering, National University of Singapore, Singapore

ARTICLE INFO

Keywords:
Air–silicone oil
ECT
WMS
DP cell
Spherical cap bubble
Slug flow
Transition

ABSTRACT

Reliable and accurate prediction of the transition from spherical cap bubble to slug flow is crucial not only to the operation of industrial facilities such as the crude oil pipelines, bubble column, and nuclear reactors but also for model development for computational fluid dynamics (CFD) studies. The present paper presents a review of the transition mechanics from spherical cap bubble flow to slug flow in vertical pipes. The bubble flow was split into sub-regions, bubbles and spherical cap bubbles and the mechanisms to classify them (i.e., bubble terminal velocity and cap bubble velocity) was analysed. For now, the literature review does not present some important previous works. This paper presents an original data set of gas–silicone oil in vertical pipes to support the new findings. The experimental two-phase data classifies the flow patterns using the probability density function (PDF) and shows the important flow variables such as average void fraction, pressure gradient, slug body void fraction, liquid slug, Taylor bubble and slug unit lengths, structural velocity and frequency obtained by electrical capacitance tomography (ECT) and a wire mesh sensor (WMS).

1. Introduction

Flow patterns play very crucial roles in two-phase gas–liquid flow. Each flow pattern has specific hydrodynamic characteristics, occurrence in nature, and many applications in industries. In the industrial applications where two-phase flow exists, the task of sizing the equipment for gathering, pumping, transporting, and storing such a two-phase mixture requires the challenging task of predicting the phase distribution in the system from giving operating conditions.

The transition from bubbly to slug flow regime has drawn much attention within the past several decades, from many investigators. In the early 1960s, Radovcich and Moissis [65] proposed that the bubble to slug transition happens due to the collisions between small bubbles, with a fraction of these collisions ending in coalescence, eventually leading to bubbles which are of similar diameter to the pipe and therefore to slug flow. Bubbly flow is consequently barely a transient flow regime, which will evolve into slug flow, given a sufficiently long residence time in a pipe.

Taitel et al. [71] followed the ideas of Radovcich and Moissis [65]. They suggested that the progressive bubble coalescence is liable for the transition to slug flow. However, they indicated that a dispersed bubble flow pattern could be sustained if the equilibrium between bubble coalescence and brake-up owing to liquid turbulence is reached. Witkinson et al. [80] reported that increasing liquid viscosity inhibits bubble coalescence, suggesting that overall void fraction is expected to increase with increasing liquid viscosity. Bousman et al. [20] stated that the bubble-slug flow regime transition is influenced by the liquid's physical properties (liquid viscosity and surface tension). Thus, implying high dominance of the transition by bubble-induced turbulence. However, Song et al. [69] and Azzopardi [15], amongst others, have suggested that the Taitel et al. [71]'s critical void fraction is a function of the ratio of average bubble diameter to the pipe diameter.

Zhang et al. [82] proposed a new mechanism for the transition from bubbly to slug flow regime using air–water as the system fluid. They established that their proposed model shows reasonably good agreement with their present experimental data. Wang et al. [78], using a four-sensor conductivity probe, reported that the bubbly to slug flow transition depends on the void fraction and significantly depends on the mixture velocity. Despite tremendous knowledge about the bubbly to

* Corresponding author.
E-mail address: mukhau@futminna.edu.ng (M. Abdulkadir).

https://doi.org/10.1016/j.expthermflusci.2021.110349
Received 8 July 2020; Received in revised form 2 January 2021; Accepted 10 January 2021
Available online 6 February 2021

Nomenclature

Symbol	Description, Units
C_0	Distribution coefficient, dimensionless
df	Pipe diameter, mSlug/plug frequency, Hz
g	Gravity constant, 9.81 m/s^2
U_m	Mixture velocity, m/s
U_T	Structure velocity, m/s
U_{SG}	Gas superficial velocity, m/s
U_{SL}	Liquid superficial velocity, m/s
V_{gd}	Drift velocity, m/s
ΔP	Pressure gradient, Pa
x	Input no-slip liquid holdup,$x = \frac{U_{SL}}{U_{SL}+U_{SG}}$
ε	Average void fraction
ρ	Density,kg/m^3
$\mu\nu$	Viscosity, kg/msKinematic viscosity, m^2/s
σL	Surface tension, N/mLength, m

Dimensionless numbers

Eotvos number $Eo = \frac{d^2 g\rho}{\sigma}$

Inverse velocity number $N_F = \frac{d^{3/2} g^{1/2} \rho}{\mu} = \left[\frac{Eo^3}{Mo}\right]^{0.25}$

Morton number $Mo = (g\mu^4)/(\rho\sigma^3)$

Froude number $Fr = \frac{U_o}{\sqrt{gd}}$

Strouhal Number $St = \frac{fD}{U_{SL}}$

Input no-slip liquid holdup $x = \frac{U_{SL}}{U_{SL}+U_{SG}}$

Subscripts

G	Gas phase
L	Liquid phase
M	Mixture
SU	Slug unit
S	Liquid slug
TB	Taylor bubble

slug flow regime, the understanding of the transition to slug flow from the spherical cap bubble flow is still quite limited and has received little attention from researchers except for efforts on either spherical cap bubble or slug flow regimes.

The first detailed documented attempt to understand the steady motion of a spherical cap bubble shown in Fig. 1 is due to Davies and Taylor [27]. They relate the bubble velocity, U_o, to the radius of curvature R of the frontal surface by a semiempirical relation true for both laminar and turbulent wakes,

$$U_o^2 = \left(\frac{4}{9}\right) gRU_o^2 = \left(\frac{4}{9}\right) gR \tag{1}$$

These authors derived equation (1) by assuming that a constant pressure exists within the bubble, and that the dynamic forces along the front surface must be balanced by gravity. Though the physical model used by these authors, according to Parlange [61] and Harper [38], appears unrealistic, it is interesting that their results agree well with experiments when the wake is turbulent.

According to Bachelor [16], the striking peculiarity of the Davies and Taylor [27] analysis is the derivation of the bubble's velocity in terms of the bubble shape. Without necessitating a reflection on the retarding force's mechanism, which balances the buoyancy force's effect on a bubble steady motion. Joseph [47] continued Davies and Taylor's [27] analysis based on inviscid potential flow to viscous potential flow. He concluded that surface tension entered the formula for the rise velocity solely when the axisymmetric bubble is not spherical. An intriguing past note is that Exner [31], one of the pioneer authors of spherical cap bubbles rising in a lake, suggested a relation

$U_o \sqrt{gR}$. Furthermore, Siemes [68] claims to have discovered the origin of equation (1) in Prandtl's unpublished notes.

For now, there is no reported work to the best of our knowledge on the transition from spherical cap bubble to slug flow regime. This transition, which is accompanied by significant changes in interfacial structure, bubble size, pressure, heat, and mass transfer, widely takes place in the chemical, petroleum, biological, and nuclear processes. There is a need, therefore, to predict the flow behaviours inherent in these flow systems in more industry-related fluids. The prediction of these flow behaviours, which is crucial to gas–liquid flow modelling, is dependent on a good understanding of the mechanism of the transition to slug flow from the spherical cap bubble. According to Taitel et al. [71] and Das and Pattanayak [24], an accurate estimation of the transition boundary is necessary to distinguish the flow structure and characteristics and to build constitutive equations. Also, the specifics of the physical mechanisms involved in the transition process are of significance for a more solid prediction of flow regimes.

The purpose of this work, therefore, is the experimental investigation of the characteristics of the transition from spherical cap bubble to slug flow using industry related fluid, air–silicone oil in a 6 m high and 0.067 m internal diameter vertical pipe. A rigorous experimental campaign was carried out to quantify the cross-sectional and radial void fractions and pressure drops by utilising the electrical capacitance tomography (ECT), wire mesh sensor (WMS) and differential pressure transducer (DP cell). The selected ranges of liquid and gas superficial velocities lie in 0.05–0.52 m/s and 0.05–4.74 m/s, respectively. Modified transition boundary models based on Taitel et al. [71] and Kaya et al. [48] were employed to develop flow maps.

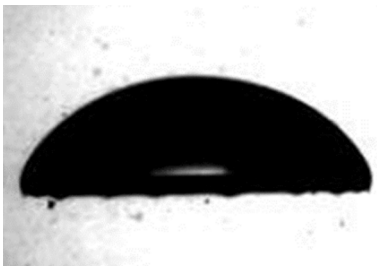

Fig. 1. Picture of a single spherical cap bubble [52].

2. Literature review

The prediction of flow attribute in two or multiple phases flowing in a pipe is more complex and challenging than in single-phase flow. The flow pattern, representing the actual arrangement of the flowing phases in the pipe, is the common distinguishing feature of multiphase flow.

2.1. Flow patterns identification

The flow regimes can be recognised by a characteristic configurational pattern of the phases in the pipe since every flow regime displays a distinctive three-dimensional arrangement of the boundary surface(s). Shoham [67] tried to establish an agreeable collection of flow regimes based on experimental data gathered across the whole spectrum of pipe inclination angles, including inclined flows, vertical-upward flow, upward and downward vertical flows, vertical-downward flow, horizontal-upward, and horizontal-downward flow. The acceptable sets of flow regimes according to Shoham [67] for the vertical flow are bubbly, slug, churn, and annular flows.

2.1.1. Bubble flow

In vertical-upward pipes with reasonably large diameters, bubbly flow is distinguished by a regularly dispersed gas phase and distinct bubbles in a liquid continuum. The number of bubbles increases with an increase in the gas flow rate, and as a result, collisions between the bubbles occur more often and account for a rise in the observed bubble coalescence. Griffith and Wallis [34] proposed that the bubble/slug transition happened at a void fraction of about 0.25–0.30.

Classification may also be categorised into a bubble or non-uniform (dispersed)-bubble flows depending on whether the magnitude of the slip velocity of the two phases. The distinct (discrete) bubbles happen in two various forms, i.e., spherical bubbles, and spherical cap bubbles. The spherical bubbles are known to be extremely small, 3 to 5 mm in diameter, and exhibit an upward zig-zag motion while the spherical cap bubbles are in relation with an upward rectilinear motion with an attendant faster rise velocity. Owing to the presence of slippage between the two phases, comparatively fewer and bigger bubbles migrate quicker than the liquid. The bubbles are also considered regular in dimension and migrate in an organized manner with a restricted number of impacts among them. However, the liquid phase is moderately agitated by the bubbles. Provided one condition, equation (2), is satisfied. The bubbly flow pattern can exist just at low liquid velocities where bubble breakup does not happen due to liquid turbulence.

1. A minimum pipe diameter criterion is founded from the comparison between the rising flow rate of the Taylor bubble and a small bubble. This condition which indicates the least diameter wherein bubble flow happens as stated by Taitel et al. [71] is fulfilled in large pipe diameters when:

$$d = 19.01\left[\frac{(\rho_L - \rho_G)\sigma}{{\rho_L}^2 g}\right]^{\frac{1}{2}} \tag{2}$$

where d is the pipe diameter, σ is the surface tension, g is the value of gravitational acceleration, ρ_G and ρ_L are the gas and liquid densities, respectively.

2.1.2. Slug flow

The slug flow regime is well-known as one of the predominant complicated flow regimes with unstable attributes. As such is discriminated by a growing series of Taylor bubbles distributed by sections of liquid slugs. This flow, according to Brill and Mukherjee [21] is distinguished by a string of slug units, comprising each of liquid slug, Taylor bubble, and a liquid film flowing downwards between Taylor bubbles and the pipe wall. Griffith and Snyder (1964) split the slug unit into three regions: the wake, which consists of a short distance directly after the Taylor bubbles, the developing and the developed regions. A developing region is one in which the length of either the liquid slug or Taylor bubble changes with the pipe's length. On the other hand, either the liquid slug or Taylor bubble's size for a developed region is stable, does not change with distance. It is worth mentioning that the wake region is extremely turbulent wherein small bubbles, the gas–liquid boundaries, and droplets of liquid are truly vague. They categorized slug flow as a significant concern to piping systems because the force of the slug produces an extremely turbulent commingling region leading to high corrosion rates owing to a high void fraction. According to Abdulkadir et al. (2014a), the performance of a corrosion inhibitor in oil and gas pipelines may be decreased due to the presence of slug flow. Sun and Jepson [70] have suggested that slug flow has sections with attendant flow turbulences and strong shearing forces that could tear-off any available film-forming corrosion inhibitor and consequently corrode the surface of the pipe.

Churn flow: is a very disturbed flow of gas and liquid whereby a gas velocity increase makes the liquid slug to become unstable, leading to break-up and fall. This liquid merges with the advancing slug, which then continues its upward motion until it becomes unstable, and after which it falls once again. The oscillatory nature of the liquid flow, though not periodic and regular, are characteristic of churn flow Abdulkadir et al. [8].

Annular flow: this flow regime is characterized by a central core of fast-flowing gas and a slower moving liquid film that travels around the pipe wall. The shearing action of the gas at the gas–liquid interface produces ripples, small amplitude waves on the liquid surface. By increasing the gas and liquid flow rates beyond the critical gas and liquid flow rates, large-amplitude surges, or disturbance waves appear. The liquid is torn from the surface of these waves giving rise to drop entrainment in the gas core. The deposition of these drops keeps the liquid film on the pipe walls.

However, the distinctions between the different flow regimes are not always apparent, and transitions are challenging to observe accurately. Therefore, there is a need to interpret the transition lines as the best estimate or most likely option of where the actual transition occurs, and the flow maps applied with care.

2.2. The rise velocity of the bubbles

Dumitrescu [30] and Davies and Taylor [27] were the first to study analytically the rise velocity of bullet-shaped bubbles that occupy the larger part of the pipe cross-section. They determined that the rise velocity of the bubbles has a value of $Fr(gd)^{0.5}$ and proposed values of Fr of 0.351 and 0.328, respectively. Dumitrescu [30] showed that the constant 0.35 should be used instead of 0.328. A numerical study on the rise velocity of bubbles, according to Joseph [47], was carried out by Bolton-Stone, Robinson, and Blake [19]. They reported that the spherical cap bubbles rise only when the Eotvos number based on an equivalent spherical radius is less than 32. They concluded that an unstable toroidal bubble is formed before the breakup for higher values of Eotvos number. However, the various authors' disagreements can be due to either the equations derived from data have a narrow range of experimental parameters or formulation.

Davies and Taylor [27] analysed the rise velocity of a spherical cap bubble, considering that motion was irrotational and the liquid inviscid. They reported that the spherical cap bubbles rising in the liquid are rounded at the top and relatively flat at the bottom. They measured the bubble shape and confirmed that it admittedly had a spherical cap while rising in water. Later, Joseph [47] applied the theory of viscous potential flow to finding the rise velocity of a spherical cap bubble. He showed that the rise velocity of the bubble, U_o, is given by equation (3).

$$\frac{U}{\sqrt{gd}} = -\frac{8}{3}\frac{v}{\sqrt{gd^3}} + \frac{\sqrt{2}}{3}\left[1 + \frac{32v^2}{gd^3}\right]^{\frac{1}{2}}$$

$$\frac{U_o}{\sqrt{gd}} = -\frac{8}{3}\frac{v}{\sqrt{gd^3}} + \frac{\sqrt{2}}{3}\left[1 + \frac{32v^2}{gd^3}\right]^{\frac{1}{2}} \tag{3}$$

where,

3. Is the kinematic viscosity

White and Beardmore [79] have conducted a comprehensive experimental investigation on the rise velocity of a Taylor bubble in a category of liquids comprising a broad range of properties. They reported that three dimensionless parameters are needed to define the buoyant rise of Taylor bubbles ascending buoyantly in liquid-filled tubes in different systems. These are the:

Froude number:

$$Fr = \frac{U_o}{\sqrt{gd}} \tag{4}$$

Morton number:

$$Mo = \frac{g\mu^4}{\rho\sigma^3} \tag{5}$$

Eotvos number:

$$Eo = \frac{\rho g d^2}{\sigma} \tag{6}$$

The effect of the viscous and surface tension forces is negligible in the region given$Mo < 10^{-6}$and$Eo > 100$. Bubbles are, therefore, inertially controlled and rise at their maximum velocity in vertical tubes, given by $Fr = 0.35$, and that surface tension according, to Wallis [77], plays little role in determining the slug ascent velocity.

There have been additional studies, the most extensive of which is that of Viana et al. [74], who investigated the effects of liquid viscosity, surface tension, and pipe diameter on the Froude number. They presented an equation of *Fr* established on the Eotvos number and a dimensionless inverse viscosity number, which they term the gravity Reynolds number, ($=\frac{\rho d^{3/2} g^{1/2}}{\mu} = \left[\frac{Eo^3}{Mo}\right]^{\frac{1}{4}}$). The equation presented by Viana et al. [74] has 13 empirical constants, and they concluded in their work that for bubbles rising in stagnant liquids, their equation gave accurate values of *Fr* for viscosities up to 3.8 Pa s. For a liquid that is not stagnant, that is, there are limited gas and liquid flow rates, the velocity of the Taylor bubble is determined from an additive equation whose two terms are due to the bulk motion and to the drift velocity (one that would occur in stagnant liquids). This can be written as

$$U_T = C_0(U_{SL} + U_{SG}) + PFr\sqrt{gd} \tag{7}$$

where,

$$P = \frac{0.905}{(1-\varepsilon_S)^{3.95}}$$

Nicklin et al. [58] reported a value of 1.2 for C_0 but noted that higher values were more appropriate as the flow rates decreased. Afterward, this has been addressed by Collins et al. [22]; Dukler and Fabre [29], and Guet et al. [36]. Hills [43] and Hills and Darton [44] worked on spherical cap bubbles, and Taylor bubbles flowing in large square cross-section columns and pipes. They reported that the velocities of larger bubbles were higher if they were moving through a swarm of bubbles, preferably than just liquid. They created a bubbly flow of known void fraction in their air/water experiments and then discharged a large volume of gas. The velocity of the Taylor bubble was marked to increase as the bubbly void fraction increased. Related results were achieved by Azzopardi et al. [14], who created slug flow by employing an air–water mixture at zero liquid superficial velocity in a vertical 67 mm internal diameter. The flow consisted of a slug unit; a series of Taylor bubbles distributed with liquid slugs containing small bubbles. The velocity of the Taylor bubbles again increased as the void fraction in the liquid slug increased. Unfortunately, most of these works present limitations because they involved either air–water systems, stagnant liquid, or small internal diameter pipes. This contrasts with the present experiment's situation, where continuous liquid, which has a viscosity five times more than water, has been used in a moderately large diameter pipe.

3.1. Flow regime transition

3.1.1. The bubble to slug flow transition

The bubble to slug flow transition, according to Lawrence et al. [51], occurs owing to the impacts between small bubbles. A portion of these impacts leads to merging. Matuszkiewicz et al. [54] observed that a minute localized disorder due to large values of void fractions can bring about a significant number of the bubbles to agglomerate along the pipe. Once the bubbles had agglomerated, the surface tension force was incapable of preventing the bubbles from coalescing. As a result, Taylor bubbles are formed. Based on the experimental results reported by Kelessidis and Dukler [49], the transition to slug flow from bubble flow takes place at low gas flow rate. That is when the Taylor bubbles first appear (the agglomeration point). Observed as the gas velocities increases is the normal appearance of Taylor bubbles. The size of the bubbles including its density, increases as the gas velocity rises at low liquid velocities. The bubbles lift upwards at these low liquid velocities, in an irregular meandering manner, impinging to form bigger ones. The discrete bubbles on reaching a point become so tightly bound that several impacts happen, and the rate of coalescing to produce bigger bubbles grows abruptly. The outcome is thus the transition to slug flow from the bubble flow regime.

Radovcich and Moisis [65] presented a semi-theoretical approach for the prediction of the transition to slug flow from bubble flow by proposing that the change happens when the number of impacts per second of the distinct bubbles is extremely high. They claimed that this could only happen at the void fraction around 0.30. Two years later, Griffith and Snyder (1964) reported that the transition to slug flow from bubble flow happens at a void fraction of 0.25–0.30. Taitel et al. [71] established the circumstances leading to the change to slug flow from bubbly. Their hypothesis was founded on examining the maximum distance of keeping bubbles unfettered moving. They stated that it occurs if the void fraction surpasses a critical $\varepsilon_c$value of 0.25 by assuming that the bubbles are spherical and ordered in a cubic framework. Venkateswararao et al. [75], two years later, applied comparable reasoning to acquire 0.25 for the value of the transition from bubbly to slug flow within a rod bundle. Their experimental data was in good agreement with the developed model. They found that when the liquid velocities are sufficiently low, the small bubbles breakup owing to liquid turbulence. Later, Mishima and Ishii [55] showed based on a semi-theoretical method, the transition to slug flow from bubble happens at a cross-sectional void fraction of 0.3. However, it is a well-established fact that the flow patterns in relatively large diameter pipes are remarkably different from those of smaller pipes Omebere-Iyari et al. [59].

Kedoush and Al-Khatab [50] investigated air–water flow patterns within a 0.038 m internal diameter vertical pipe. Kedoush and Al-Khatab [50] found that the evolution to slug flow from bubble flow happens at $\varepsilon = 0.30$ and that slug flow arises in the range $0.3 \leq \varepsilon \leq 0.7$. A decade later, Kaya et al. [48] also proposed a new model for this transition boundary based on their new bubble slip velocity formulation. The transition equation expressed in terms of superficial velocities is shown in equation (8).

$$U_{SG} = 0.333U_{SL} + 0.3825\left[\frac{g(\rho_L - \rho_G)\sigma}{\rho_L^2}\right]^{\frac{1}{4}}\sqrt{Sin\alpha} \tag{8}$$

Guet et al. [35] showed in their work that the transition to slug flow from bubbly flow is greatly reliant on the inlet pipe arrangement, especially on the size of the bubbles. They claimed that fluid properties like the densities of the two phases, surface tension, and the viscosities of the two phases are essential variables in determining the process of the bubbly-slug transformation. The variables are known to influence the commingling actions between bubbles and the structure velocity of the bubbles. According to Omebere-Iyari and Azzopardi [59], the dynamic surface tension, initial bubble size and velocity, purity, and pipe internal diameter are the ones that may change the flow behaviour significantly when varied.

3.1.2. Spherical cap bubble transition

As reported in Gao et al. (2014), the transition to slug flow from bubbly flow pattern is described by the uneven spread of small bubbles in the direction of flow. Gao et al. (2014) claimed that the evolution to slug flow from bubbly flow is distinguished by a global agglomeration of small bubbles that leads to the creation of a cap-like bubble that hastens the flow transition to complete. The procedure dictating the transition to slug flow from bubbly is the formation of a cap that is formed after an adequate number of small bubbles coalesce. Hence, the cap bubbles are

not actually responsible for the formation of slug flow. Nevertheless, at relatively higher gas velocities (though still low), the bubble density rises, promoting more impacts and coalescences and eventually leading to the creation of Taylor bubbles. The created Taylor bubbles envelop fully cross-sectional area of the pipe. According to Shoham [67], this establishes the transition to slug flow from bubble flow. These bubbles, however, can produce a strong secondary flow impact. They follow a straight-line path with some base alternations. With these bubbles, the inertial effect of flow enveloping the bubbles prevails. Simultaneously, the influence of surface tension, viscosity, and impurities of the liquid medium are inconsequential.

Based on the detailed literature review, there is scant knowledge on the transition from spherical cap bubble to slug flow regime and it is also clear from the results of the air–water multiphase studies presented above that there are many parameters that influence the transition from the spherical cap bubble to slug flow regime. Such parameters are translational bubble (structure) velocity, frequency, void fraction in the liquid slug, void fraction in the Taylor bubble, pressure drop, liquid slug, Taylor bubble, and the slug unit lengths. It is expected when the model fluids are changed; the two-phase transition from the spherical cap bubble to slug flow regime behaviour will be different. Therefore, to characterize the conditions that result in the onset of the transition from the spherical cap bubble to slug flow regime in more industry relevant fluids, an experimental study was conducted using air and silicone oil flow in a vertical pipe. The present research aims to fill the gap in understanding the characteristics of the transition from the spherical cap bubble to slug flow regime.

4. Experimental setup

4.1. Experimental facility

All the work reported here was carried out on an inclinable facility, which was kept vertically for this task. The 6 m long vertical test pipe has an internal diameter of 0.067 m. The system fluids mixture under investigation is air–silicone oil, supplied at the bottom of the pipe. Silicone oil is an excellent insulator and has a viscosity ~ 0.005 mPa.s. More details about the rig can be found in Hernandez-Perez [40] and Abdulkadir [1]. Fig. 2 displays a diagram of the flow loop. The chosen superficial velocities for air and liquid were from 0.05 to 4.74 m/s and 0.05 to 0.52 m/s, respectively. Table 1 shows the locations of the measurement instruments along the pipe. The experimental data were simultaneously recorded in a single campaign. (See Table 2)

Air and liquid were combined at the base of the pipe via a goal-designed gas–liquid homogenising chamber (Fig. 3). Several investigators have described several different mixers for two-phase flow.

Table 1
Position of the ECT, WMS and DP cell on the measurement sections of the pipe.

	Plane 1 of the ECT	Plane 2 of the ECT	WMS
Position from the gas–liquid mixing unit (m)	4.4	4.489	4.92
Flow development length	66	67	73

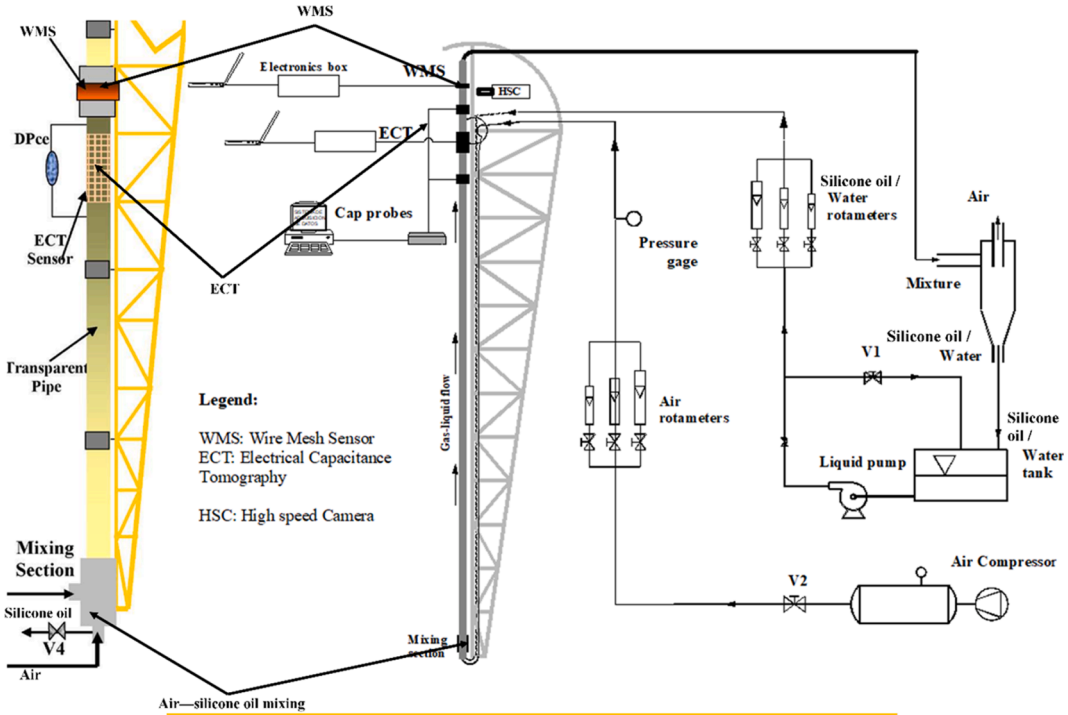

Measuring instrument	Distance from the mixing section (m)
Electrical capacitance tomography (ECT) plane 1	4.40
Electrical capacitance tomography (ECT) plane 2	4.489
Differential pressure transducer (DP cell) 1	4.00
Differential pressure transducer (DP cell) 2	4.86
Wire mesh sensor (WMS)	4.92

Fig. 2. Schematic representation the experimental rig employed in this research.

Table 2
Properties of the air–silicone oil and dimensionless numbers at 1 atm and at the operating temperature of 20 ± 0.5°C.

Silicone oil						
Pipe internal diameter (mm)	Viscosity (kg/ms)	Density (kg/m^3)	Surface tension (N/m)	Eotvos number (*Eo*)	Morton Number (*Mo*)	Gravity Reynolds number (N_f)
67	0.005	900	0.02	1982	1.0325*10^{-6}	9312
Air						
Density (kg/m^3)	Temperature (°C)	Pressure (atm)	Viscosity (kg/ms)			
1.2	20	1	0.0000181			

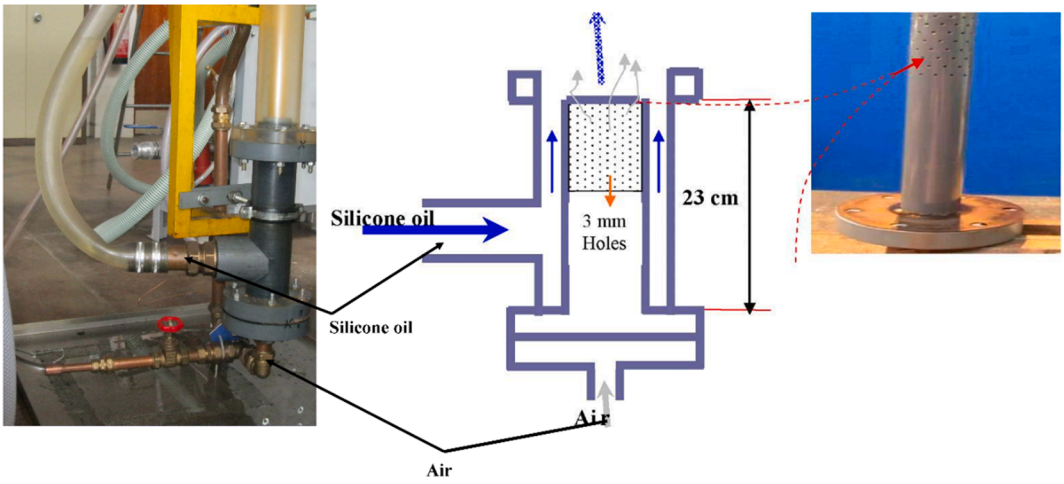

Fig. 3. Gas–liquid air–silicone oil mixing chamber.

Often dictated is the choice of mixer geometry by the flow pattern that is of primary interest. For an investigation covering a whole range of flow patterns, of which the present study is an example, Govier et al. [32] determined that the mixing section's geometry affects the flow pattern, only for a very short distance. They concluded that with an adequate calming section, a simple "tee" was suitable. The concept of Govier et al. [32] was adopted in this work by ensuring that the mixing of the air and silicone oil phases took place in such a way as to reduce flow instability. Flow stability was achieved using a purpose-built mixing unit (annular section). The mixing unit shown in Fig. 3 was made from polyvinyl chloride (PVC), providing the maximum time for the two-phases to develop. The silicone oil arrived at the homogenising (mixing) compartment from a side and flowed about a honeycombed drum. Air also entered the homogenising chamber via a vast number of 3 mm-diameter holes. Hence, the air and liquid became mixed at the entrance to the pipe. A set of rotameters was utilised to establish the inlet air and silicone oil volumetric flow rates.

Numerous experimental runs were conducted with air–silicone oil mixture in this rig to create and develop as many flow patterns as possible. Table 3 shows the range of liquid and gas superficial velocities deployed in this work. Total 91 sets of experimental conditions were included in the measuring matrix. The flow pattern boundary lines reported in Pereyra and Torres [62] are used to delineate the flow conditions into their respective flow regimes for ease of flow pattern identification. The spherical cap bubble, slug, and churn flow are the marked flow regimes in the whole experimental campaign. However, the flow regimes under consideration in this work are spherical cap bubble and slug flows only.

(See Table 4)

Positioned at 4.40 m from the gas–liquid mixing inlet was the ECT plane 1, followed shortly by the ECT plane 2. The WMS was situated at 4.92 m from the gas–liquid mixing inlet. This arrangement avoids any possible intrusive effect from WMS on the flow to ECT measurement. The use of the three instrumentation was supplemented with a high-speed video camera to capture the flow behaviour.

The experimental data reported here refers to conditions in which the rise velocity of the bubble is determined solely by liquid inertia. According to Wallis [77], this regime corresponds to$Eo > 100$ and$N_f > 300$. The physical properties of the air–silicone oil system and the values of the dimensionless numbers,*Eo*, *Mo*, andN_f are presented in Table 2. Table 3 shows the measurement degree of uncertainty.

Table 3
Measurement degree of uncertainty.

Measured parameters	Degree of uncertainty (±)
Temperature (°C)	0.5
Pressure drop (N/m^2)	0.44 of scale
Volumetric flux of the liquid (m/s)	10% [6]
Volumetric flux of the gas (m/s)	7–22% [3]
Liquid holdup/void fraction obtained using the ECT	less than 5% [45] and Hansen et al. [37]
Void fraction/liquid holdup obtained using the WMS	less than10% [25]

4.2. Electrical capacitance tomography (ECT)

ECT measurement is based on detecting the relative permittivity difference from different phases. It is non-intrusive to the fluids. It was successfully employed for liquid–liquid flow [39], gas–solid flow [13] and more recently gas–liquid flow Marashdeh [53,9,9] Pradeep et al. [63,4–5,6,3] , Mohammed et al. [56], and [8]. The ECT system (Tomoflow R100) used in this work comprises of a measurement circuitry, capacitance sensor, and a data acquisition computer as stated in Abdullahi et al. [12]. The ECT encompasses an array of same-sized electrodes made by using a flexible Printed Circuit Board (PCB) technology [12].

Fig. 4(a-b) shows the photograph of an ECT with eight electrodes arranged externally around a non-electrically conductive pipe. Each electrode is 35 mm in length and 26.4 mm in breadth. The ECT comprises two measuring planes with 89 mm apart axially between their centres. Guard electrodes were installed on both sides of the measurement electrodes to minimize signal noise [12].

Table 4
The employed series of parameters in the present work.

U_{SL}(m/s)	U_{SG} (m/s)	ε	Absolute accuracy error	Relative error (%)	Re_{SL}	Re_{SG}
0.05–0.52	0.05–4.74	0.13–0.64	0.012 to 0.020	1.1 to 3	603–6271	222–21,055

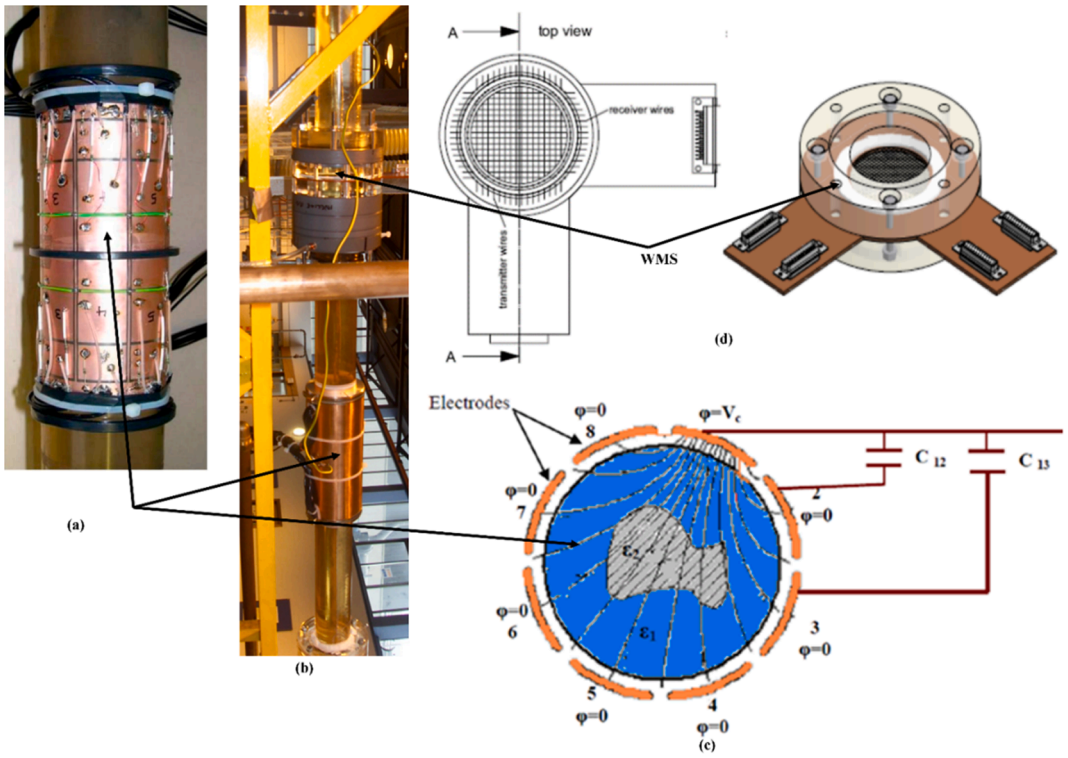

Fig. 4. Instrumentation employed in this work using (a) Photo of the ECT sensor Faraday cage (b) Photo of the ECT wrapped around the pipe (c) Operation principle of an eight electrode ECT sensor and (d) WMS (2X24 electrode wires).

The system normalises the permittivity of air (empty pipe) and silicone oil (full liquid) as 0 and 1, respectively. Fig. 4c illustrates the measurement principle of an ECT with eight electrodes in a cross-sectional view. The electrodes according to Abdulkareem [10] are excited one by one in a single measurement period while maintaining the others at a reference potential. The void fraction is determined by the capacitance obtained from electrode duos. The measurement error of the ECT, according to Huang et al. [45] and Hansen et al. [37], is less than 5%, which they obtained by comparing the measured value of the void fraction against the real void fraction value.

4.3. Capacitance wire mesh sensor (WMS)

Like the ECT, the measurement concept of the WMS is founded on the difference in relative permittivity of the two phases available in the pipe. The capacitance WMS measures the instantaneous local permittivity distribution of the flowing air and silicone oil mixture in the pipe. The sensor was specially designed in this work to fit the test pipe and situated at 4.92 m from the air–silicone oil mixing section. The capacitance WMS according to Abdulkareem et al. [11]) is made up of two planes with each having 24 stainless steel wires. The wires have diameter of 0.12 mm. The planes are separated by a 2 mm gap. Within one plane, the distance between neighbour wires is 2.8 mm. An electronics box contains the circuitry that measures the permittivity across the shortest distance between two perpendicular wires using a multiplexed excitation-probing scheme. The WMS is made into an acrylic resin support, which allows it to be fixed in the test pipe. Fig. 4d displays a photo of the WMS. It was successfully employed for gas–liquid flow by da Silva et al. [26],Azzopardi et al., [13,9,5] , Vuong et al. [76],Shaban et al. [66], Zhao et al. [81], Tompkins et al. [72], Prasser and Hafeli [64,3,2,8] .

To determine the uncertainty of the WMS instrument, da Silva [25] estimated the relative deviation from a reference value and maximal deviation from the average permittivity value using equations (9) and (10), respectively. He found that the relative deviation from the average permittivity and maximal deviation from the average permittivity value to be less than 10%.

$$\beta = \frac{\overline{\varepsilon} - \epsilon^{ref}}{\varepsilon^{ref}} \tag{9}$$

$$\gamma = \max_{\forall i,\forall j}\left[\frac{\overline{\varepsilon} - \varepsilon(i,j)}{\overline{\varepsilon}}\right] \tag{10}$$

Where

β is the relative deviation from a reference value

γ is the relative deviation from the average permittivity value for silicone oil

$\overline{\varepsilon}$ is the average value of permittivity of all crossing points and is determined from equation (11)

$$\overline{\varepsilon} = \frac{1}{256}\sum_{i=1}^{16}\sum_{j=1}^{16}\varepsilon(i,j) \tag{11}$$

and $\varepsilon(i,j)$ is the measured permittivity distribution for silicone oil.

The detailed description of this instrument can be in da Silva et al. [26] and Abdulkadir et al. [5].

4.4. Methodology of data analysis

The Probability Density Function (PDF), Power Spectral Density (PSD), Cross-correlation, and the approach developed by Abdulkadir et al. [4] for obtaining the liquid slug, Taylor bubble and slug unit lengths were executed for the analysis of the data obtained in this work. These are displayed here.

A probability density function (PDF) is the variation of the probability that the void fraction values lie within a specific range ($\varepsilon \pm \delta\varepsilon$) versus void fraction Abdulkadir [1]). It is the distribution of how often each value of void fraction occurs in a time series. The PDF was determined by counting the number of void fraction data points in data bins of width 0.01 centred on void fractions from 0.005, 0.015 …0.995, and then dividing each sum by the total number of data points. They confirm the dominant void fractions, which are observed for each flow condition. The PDF is explicitly useful, as confirmed by Costigan and Whalley [23,9;4;8] , amongst others, because it depicts different signatures for each flow pattern in vertical upward flows: bubbly flow possesses a single peak at a low void fraction; spherical cap bubble flow has a peak at a lower void fraction with a broadening tail down to higher void fractions; slug flow is characterized by two peaks, one at low void fraction signifying the liquid slug and one at higher void epitomising the Taylor bubble region; churn flow has a peak at a higher void fraction with a tail down to lower void fraction; annular flow has a single peak at a high void fraction.

To determine the frequency of periodic structures (slugs or spherical cap bubbles), the methodology of Power Spectral Density (PSD) as described by Bendat and Piersol [83] is applied. The Power Spectral Density, PSD, is a measure of how the power in a signal varies over a frequency range. Therefore, it describes how a time series' power (or variance) is distributed with frequency. It is defined as shown in equation (12) as the Fourier Transform of the time series' autocorrelation sequence. The method presents the power spectrum density functions in terms of direct Fourier Transformations of the original data.

$$S_{ab}(f) = \int_{-\infty}^{+\infty} R_{ab}(\tau) e^{-j2\pi f\tau} d\tau \tag{12}$$

Equation (12) as given in Abdulkadir [1] is the cross-spectral density function between *a (t)* and *b (t)*. For the special case where *a (t) = b (t),*

$$S_{ab}(f) = \int_{-\infty}^{+\infty} R_{bb}(\tau) e^{-j2\pi f\tau} d\tau \tag{13}$$

Equation (13) represents the power spectral density (PSD) function.

Cross-correlating the time-varying void fraction data measured by the twin ECT-planes positioned at 4.4 and 4.489 m above the mixer section at the base of the pipe. This permits the determination of the time for individual spherical cap bubbles/slugs to travel between the two ECT-planes. The axial distance, which is 0.089 m (=4.489–4.4), was used to divide the obtained time, and hence produces the structure velocity, U_T.

The PDF of the void fraction as noted above, for slug flow, is distinguished by two peaks. The one at a lower void fraction, ε_S, corresponds to the liquid slug. The higher value peak at ε_{TB} relates to the Taylor bubble.

The length of a slug unit is obtained from the knowledge of the translational velocity of the Taylor bubbles (structure velocity) and the spherical cap bubble/slug frequency shown using equation (24). A slug unit is a Taylor bubble and the resulting liquid slug. The lengths of the different regions of the individual slug unit have been determined for the range of liquid and gas superficial velocities. The times of passage of the individual slug unit, Taylor bubble, and the liquid slug have been determined from an analysis of the time series of the void fraction recorded from the twin-planes of the ECT signals. The times of passage for the slug unit, the Taylor bubble, and the liquid slug were then assumed to be proportional to the lengths of the slug unit, Taylor bubble, and liquid slug, respectively. An establishment of relationships to estimate the lengths of the individual Taylor bubble and the liquid slug, as described below, were built based on some valid assumptions.

Assumptions:. 1. *The spherical cap bubble/slug/Taylor bubble are uniform, $\theta = \frac{1}{f}$where, f is the spherical cap bubble/slug frequency.*

2. Steady state so that the front and back of the slug have the same velocity

where, $\theta$is a time for a slug unit to pass the ECT

Therefore,

$$U_T = \frac{L_{SU}}{\theta} \tag{14}$$

where, $\theta$is a time for a slug unit to pass the ECT

Therefore,

$$L_{SU} = \frac{U_T}{f} \tag{15}$$

For an individual slug unit,

$$L_{SUi} = kt_{SUi} \tag{16}$$

$$L_{TBi} = U_{Ti} t_{TBi} \tag{17}$$

$$L_{Si} = U_{Ti} t_{Si} \tag{18}$$

Dividing equation (18) by (17) yields the expression

$$\frac{L_{Si}}{L_{TBi}} = \frac{U_{Ni} t_{Si}}{U_{Ni} t_{TBi}} = c$$

$$\frac{L_{Si}}{L_{TBi}} = \frac{U_{Ti} t_{Si}}{U_{Ti} t_{TBi}} = c \tag{19}$$

$$L_{si} = cL_{TBi} \tag{20}$$

Nevertheless,

$$L_{SUi} = L_{TBi} + L_{Si} \tag{21}$$

Substituting equation (20) into (21) and rearranging yields the expressions

$$L_{SUi} = L_{TBi} + cL_{TBi} = L_{TBi}(1 + c) \tag{22}$$

$$L_{TBi} = \frac{L_{SUi}}{1 + c} \tag{23}$$

$$L_{Si} = L_{SUi} - L_{TBi} \tag{24}$$

Equations (15), (23), and (24) were employed to determine the slug unit, Taylor bubble and liquid slug, respectively.

4.5. Results and discussion

The corresponding flow regime map created employing the FLOPATN computer code established by Pereyra and Torres [62] is displayed in Fig. 5.

4.6. Validation of the ECT data using WMS data

The ECT in this work provides comprehensive information about gas–liquid flows, whereas the WMS verifies the accuracy of void fraction measurements. In each run, cross-sectional void fractions were simultaneously measured by ECT and WMS. The data requisition of WMS was activated by the signal from the ECT data collection trigger. Fig. 6 compares the results from the two measurement methods. Previously published in Azzopardi et al. [13]), Abdulkareem [10]), and [9,5;3] is

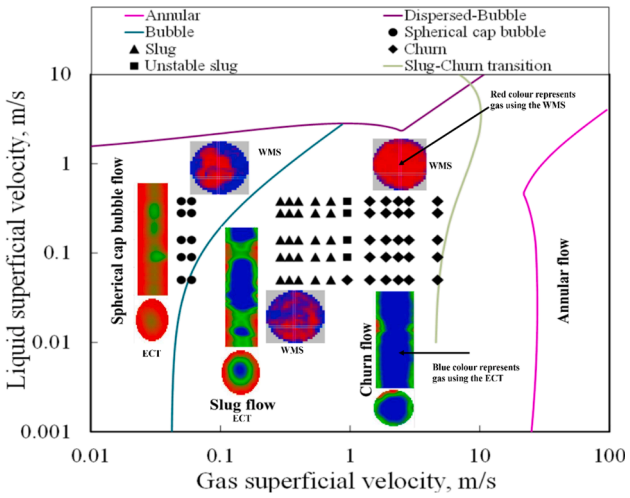

Fig. 5. Flow pattern map of Pereyra and Torres [62] showing the flow patterns determined from PDFs in the present experiments. The flow patterns under consideration in this work are spherical cap bubble and slug transition flow. The ECT output represents blue colour as gas while the WMS output depicts red as gas. (For interpretation of the references to colour in this figure legend, the reader is referred to the web version of this article.)

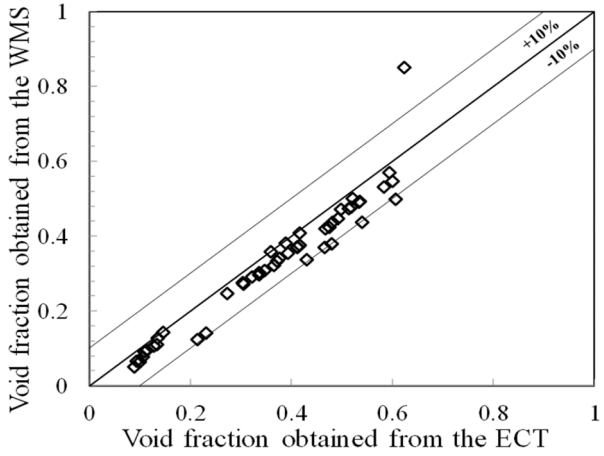

Fig. 6. Cross-plot for comparison between the ECT and WMS.

the comparison between ECT and WMS measurements. In general, the values from the ECT are bigger than those from WMS but the difference is within±10%. The disagreement may be partially attributed to the intrusiveness of WMS.

4.7. Probability density function (PDF) for flow pattern recognition and frequency determination by the power spectral density (PSD) approach

4.7.1. Probability density function (PDF) for flow pattern recognition

The PDF of void fraction is regarded as a valuable and objective procedure for distinguishing flow patterns. Costigan and Whalley [23] and Abdulkadir et al. [8] revealed that each common flow pattern has a unique feature on its PDF of void fractions. According to Abdulkadir et al. [8], the PDF of void fraction for spherical cap bubble flow has a single peak at a low void fraction followed by a broadening end while the plot of slug flow has dual peaks appearing at low and higher void fractions. Following the PDF approach of Costigan and Whalley [23] and Abdulkadir et al. [8],Fig. 7(a, c, e) defines the spherical cap bubble flow whereas, Fig. 7(b, d, f) denotes slug flow. The values of the average cross-sectional void fraction are boldly shown in Fig. 7(a–f).

An increase in gas superficial velocity from 0.05 m/s, the first column (Fig. 7(a, c, e)) to 0.40 m/s, the second column (Fig. 7(b, d, f), the spherical cap bubble flow changes to slug flow. A closer look at Fig. 7a reveals that the widening tail that is noticeable in the spherical cap bubble flow regime diminishes with an increase in the liquid superficial velocity. Fig. 7e shows that at the liquid superficial velocity of 0.38 m/s, the PDF of void fraction exhibits a single peak at a low void fraction because the spherical cap bubble flow abruptly changes into the bubble flow regime. There are two competing mechanisms likely responsible for this behaviour. Firstly, the liquid superficial velocity of 0.38 m/s is sufficient to cause the liquid turbulence to be superior to the bubble coalescence mechanism, and as a result, the spherical cap bubbles collapse into discrete bubbles. Secondly, the surface tension force prevented the bubbles from coalescing into larger ones, and consequently, the spherical cap bubble flow becomes a bubble flow regime.

Also, the large-size Taylor bubble shown in Fig. 7b collapses with an increase in the liquid superficial velocity. The shrinkage of the widening tail of the spherical cap bubble flow regime and the collapse of the big-size Taylor bubbles can be related to the superiority of the high degree of liquid turbulence in comparison to the bubble buoyancy force. As a result, the gas is dispersed as distinct small bubbles in a continuous liquid flow. The results conform with the observations of Radovcich and Moisis [65]; they claimed that the break-up of bubbles owing to liquid turbulence is a key for the slug to bubble flow transition and that this happens when the void fraction > 0.2. These observations are confirmed by visual inspection and the contours of phase distributions shown in Fig. 7(a–h) obtained from the WMS.

4.7.2. Frequency determination by the power spectral density (PSD) approach:

The PSD approach was employed for the determination of periodic structure frequency. The PSD according to Abdulkadir [1] illustrates whence the power of a time trace of a void fraction is spread with the frequency. Also, a plot of PSD against frequency helps depict how the flow pattern changes with the liquid and gas superficial velocities by the feature of the curve. The frequency can be obtained from the peak of its PSD.

Fig. 8(a–h) shows the plots of PSD against frequency and the corresponding plots of time series of the void fraction at various liquid and gas superficial velocities. Also, the influence of the liquid superficial velocity on the frequency is determined. The values of the dominant frequency are boldly shown in Fig. 8(a–h).

Fig. 8 (a, c, e, g) shows several distinct peaks with each peak corresponding to a frequency that can be observed in the PSD plots for the spherical cap bubble flow. For the slug flow regime presented in Fig. 8 (b, d, f, h), the PSD plot shows some peaks that are not as obvious as those of the spherical cap bubble flow. Table 5 presents the details of the number of principal peaks, including the frequency corresponding to each peak and classification. A similar observation witnessed in the spherical cap bubble flow PSD plots is also seen in the PSD plots for the slug flow regime, the frequency amplifies with an increase in the liquid superficial velocity.

Observed from Fig. 8a at the liquid and gas superficial velocities of 0.05 and 0.05 m/s, respectively, are three principal peaks that occur at frequencies of 1.8, 2.8, and 3.8 Hz. The frequencies of the three observed peaks can be regarded as harmonics because the frequencies are periodic at 1 Hz. The number of peaks shown in Fig. 8(a, c, e, g) and summarised in Table 5 increases in an arithmetic progression from 3 to 5, 7, and finally 9 with an increase in the liquid superficial velocity. Table 5 shows the values of frequencies corresponding to each peak in the PSD plot. The values of the dominant frequency, on the other hand, are boldly shown in Fig. 8(a, c, e, g) and increases from 1.27 to 1.7 Hz with an increase in the liquid superficial velocity for the spherical cap bubble flow regime. Similarly, for the slug flow regime, the values of the dominant frequency are displayed boldly in Fig. 8(b, d, f, h) and increases from 1.7 to 3.1 Hz with an increase in the liquid superficial velocity. In conclusion, the liquid superficial velocity has a remarkable

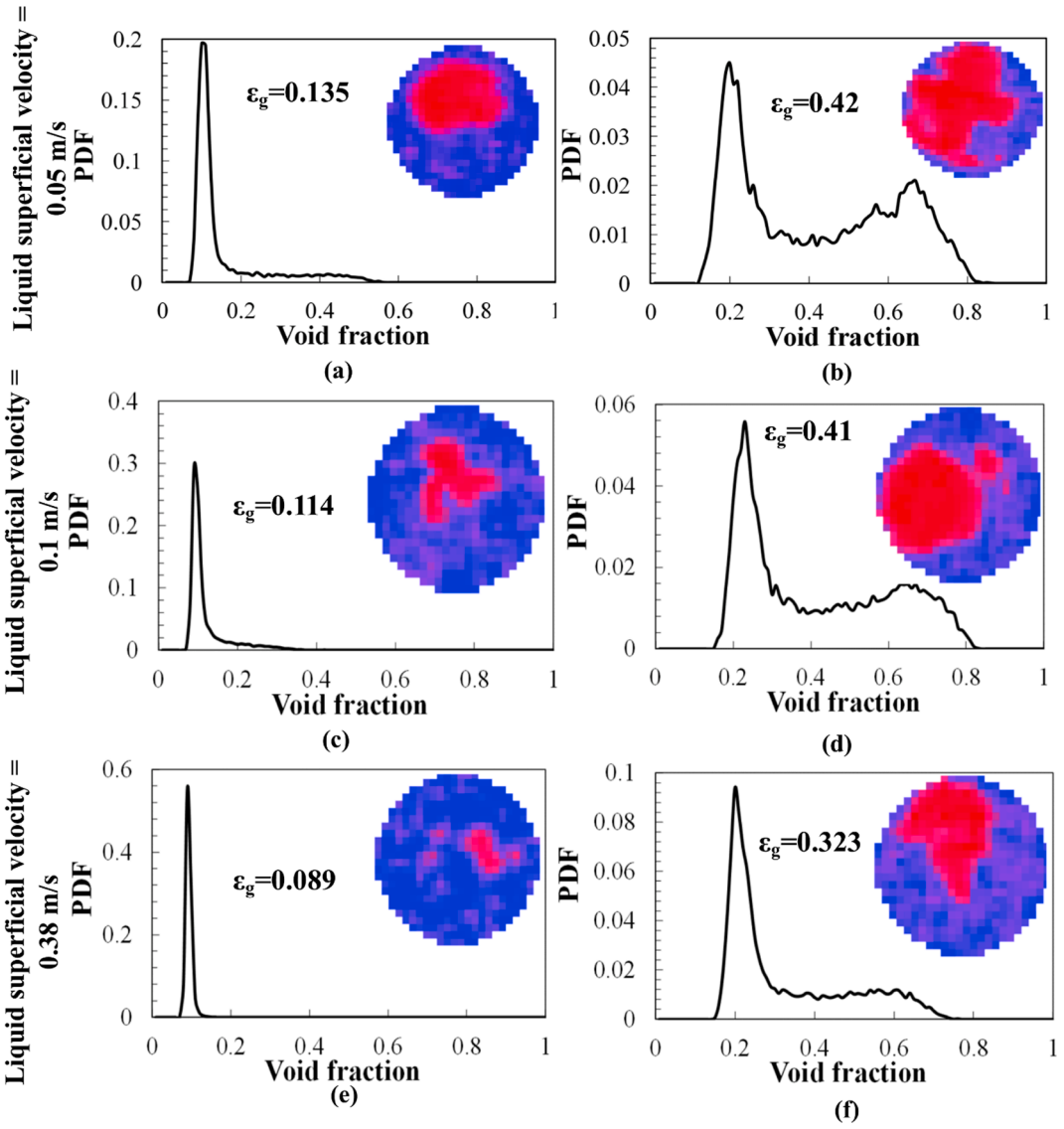

Fig. 7. PDFs of void fraction time series. Also, embedded in the graphs are the profiles (contours) of the gas and liquid phases and are depicted by red and blue colours, respectively. First column (a, c, e): gas superficial velocity is 0.05 m/s. Second column (b, d, f): gas superficial velocity is 0.40 m/s. The liquid superficial velocities (m/s) are: (a) 0.05 (b) 0.05 (c) 0.1 (d) 0.1 (e) 0.38 (f) 0.38. The bold void fraction represents the average cross-sectional void fraction. (For interpretation of the references to colour in this figure legend, the reader is referred to the web version of this article.)

effect on the number of principal peaks and the dominant frequency.

With an increase in gas superficial velocity to 0.40 m/s displayed in Fig. 8(b, d, f, h), the PSD plot reveals two peaks, which grow with an increase in the liquid superficial velocity. The observed peaks, however, cannot be regarded as harmonics, but perhaps the frequencies of the two classes of structures, the liquid slug and Taylor bubble, seen in the embedded time traces of void fraction.

Fig. 8(a–h), based on the embedded time traces of the void fraction, reveals that owing to an increase in the number and size of bubbles approached is the slug flow regime from the spherical cap bubble flow as the gas superficial velocity increases from 0.05 to 0.40 m/s. According to Griffith and Wallis [34], the bubble to slug transition flow happens at the void fraction of 0.25–0.30. At gas superficial velocity of 0.4 m/s, the spherical cap bubbles in Fig. 8(a, c, e, g) combine with other smaller-sized bubbles (agglomerate) to produce larger ones shown in Fig. 8(b, d, f, h). These bubbles perhaps nearly fill the entire cross-section of the pipe, leading to an increase in bubble size and void fraction. Hence, a formation of bullet-shaped Taylor bubbles segregated by liquid slugs along with some entrained small bubbles. The ensuing flow regime is a slug flow.

In conclusion, Fig. 7(a, c, e) shows that the number and size of bubbles including its density and void fraction based on the PDF tail of the spherical cap bubble, decreases with an increase in the liquid superficial velocity. This observed behaviour can be associated with the superiority of attributed to the superiority of the high liquid velocity (the flow regime is turbulent flow based on the liquid phase Reynolds number) which subdued the surface tension forces that keeps the large bubbles together. Consequently, the bubbles are broken down into smaller ones, leading to the formation of bubbly flow regime. The observed trend is corroborated by the PSD plots in Fig. 8(a, c, e, g) that owing to the superiority of the liquid turbulence, against the bubble coalescence, the number of peaks, including the associated frequency of the individual peaks and the dominant frequency increases with an increase in the liquid superficial velocity. According to Abdulkadir et al. [4], the dominant frequency increases with an increase in liquid superficial velocity.

Fig. 9 shows the graph of frequency versus gas superficial velocity at different liquid flow superficial velocities. At liquid superficial velocities

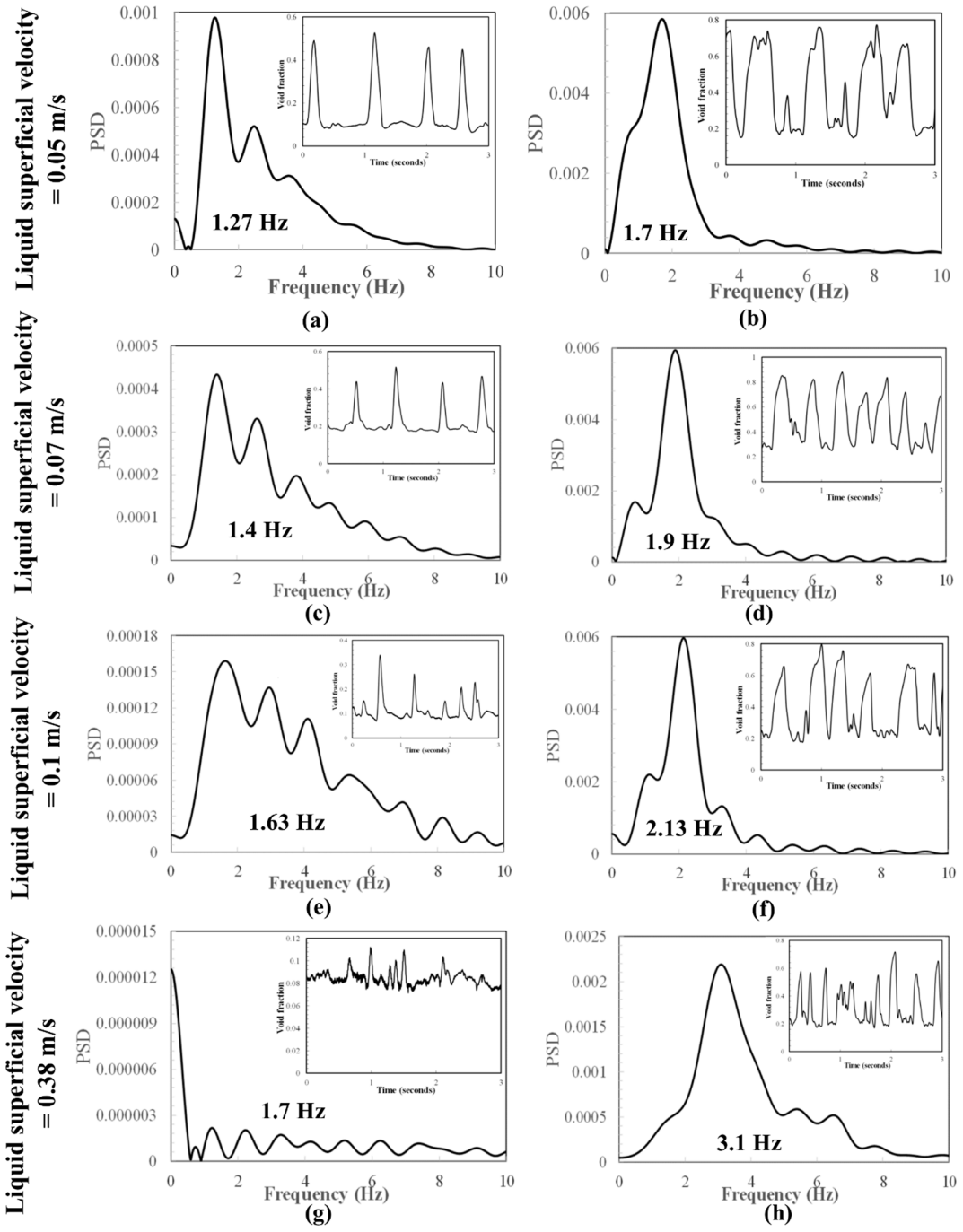

Fig. 8. Power spectral densities (PSD). Also, embedded in the graphs are the graphs of time traces of void fraction. First column (a, c, e, g): gas superficial velocity is 0.05 m/s. Second column (b, d, f, h): gas superficial velocity is 0.40 m/s. The liquid superficial velocities (m/s) are: (a) 0.05 (b) 0.05 (c) 0.07 (d) 0.07 (e) 0.1 (f) 0.1 (g) 0.38 (h) 0.38. The bold frequency represents the dominant frequency.

of 0.05, 14 and 0.28 m/s shown in Fig. 9a, the frequency generally first tends to reduce, and then rise followed by a region of relative stability wherein a moderately constant frequency is observed. The observed decrease in frequency according to Hernandez-Perez et al. [41] can be attributed to a high upward acceleration of liquid opposite the reversed liquid film at the back of a gas pocket. On the contrary, the region of moderately constant frequency may be due to the presence of a similar flow pattern. At liquid superficial velocities of 0.07, 0.1, and 0.38 m/s, no decrease in frequency is observed owing to the absence of reversed flow. Furthermore, the plots also indicate the prevailing flow patterns already identified by the PDFs.

Next in Fig. 9 (a-b), the corresponding values of the obtained dominant frequencies for all the experiments are presented.

It can be noticed in Fig. 9(a-b) that the liquid superficial velocity greatly influences the frequency of the periodic patterns of the spherical cap bubble and slug flows. According to Fig. 9(a-b), the frequency varies between 3.5 and 1.25 Hz. The frequency at the liquid superficial velocity of 0.05 m/s slightly rises with the gas superficial velocity. At 0.14 m/s, the gas superficial velocity shows a weak influence on the frequency. However, at 0.38 m/s, the frequency fluctuated with the gas superficial velocity and reached the minimum at the gas superficial velocity of 0.54 m/s.

The behaviour seen in Fig. 9a ascribed to a change in the flow pattern is also reflected in Fig. 9b. These results confirm the conclusions of

Table 5
The properties of the PSD against frequency plot.

U_{SL} (m/s)	U_{SG} (m/s)	Number of main peaks	Frequency of the individual main peaks (Hz)	Classification	Flow pattern
0.05	0.05	3	1.8, 2.8 and 3.8	Harmonics	Spherical cap bubble
0.07	0.05	5	1.7, 2.7, 3.7, 4.7 and 5.7	Harmonics	Spherical cap bubble
0.1	0.05	7	1.8, 2.8, 3.8, 4.8, 5.8, 6.8, 7.8 and 8.8	Harmonics	Spherical cap bubble
0.38	0.05	9	1.2, 2.2, 3.2, 4.2, 5.2, 6.2, 7.2, 8.2, and 9.2	Harmonics	Bubbly flow

earlier investigations in vertical slug flow, Jepson and Taylor [46] and Abdulkadir et al. [4]. Furthermore, Fig. 9a displays a maximum frequency for the spherical cap bubble flow regime.

A plot of dimensionless Strouhal number, St, against input no-slip liquid holdup, x, is used to interrogate the proportionality of frequency to liquid superficial velocity for constant pipe diameter and input no-slip liquid holdup. The St according to Abdulkadir et al. [4] represents the ratio of inertial forces owing to the instability of the flow to the inertia forces because of variations in velocity from one spot to another. The input no-slip liquid holdup, x, on the other hand, according to Abdulkadir et al. [2,8] is described as the quotient of liquid superficial velocity to the mixture velocity.

Since frequency is proportional to liquid superficial velocity, a linear graph is expected from a plot of St against x. The St and × can be represented as equations (25) and (26), respectively.

$$St = \frac{fD}{U_{SL}} \tag{25}$$

$$x = \frac{U_{SL}}{U_{SL} + U_{SG}} \tag{26}$$

Displayed in Fig. 10 is the plot of St against × on a semi-logarithmic graph. The figure reveals that the proportionality of the frequency to the liquid superficial velocity in the present work is found. The plot also shows that, in general, the relationship between frequency and liquid superficial velocity is approximately linear. Correctly predicted is the influence of the liquid superficial velocity on the frequency.

4.8. Structure velocity of the bubbles against mixture velocity

According to Nicklin et al. [58], the structure velocity of the observed flow patterns can be determined by cross correlating the time traces of liquid holdup/void fraction signals obtained from the two ECT sensors. The details of the cross-correlation approach can be found in Nicklin et al. [58] and Abdulkadir et al. [4]. A plot of the structure velocity against the mixture velocity is shown in Fig. 11.

The structure velocity of the bubbles according to Abdulkadir et al. [4] is assumed to compose of two key parts: the drift velocity and the maximum mixture velocity in the slug body. It is instructive to note that these two main components can be extracted from the graph of structure velocity, U_T, versus mixture velocity, U_M. As shown in the figure, a straight-line relation is established between the structure velocity and the mixture velocity for the spherical cap bubble and slug flow regimes. Also, the positive slopes in the two graphs indicate that the structure velocity grows with the increase of the mixture velocity. The gradient of the fitted line represents the distribution coefficient/parameter, C_0, and the intercept on the y-axis signifies the drift velocity, V_{gd}. The relationship between U_T and V_{gd} is defined in Equation (27).

$$U_T = C_0 U_M + V_{gd} \tag{27}$$

The obtained structure velocities for the spherical cap bubble and slug flows are $U_T = 1.34U_M + 0.58$ and $U_T = 1.33U_M + 0.76$,

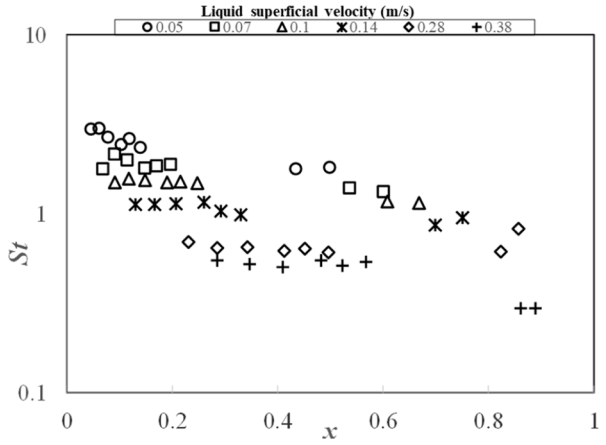

Fig. 10. Semi-logarithmic graph of the dimensionless frequency based on liquid superficial velocity against the input no-slip liquid holdup, *x*.

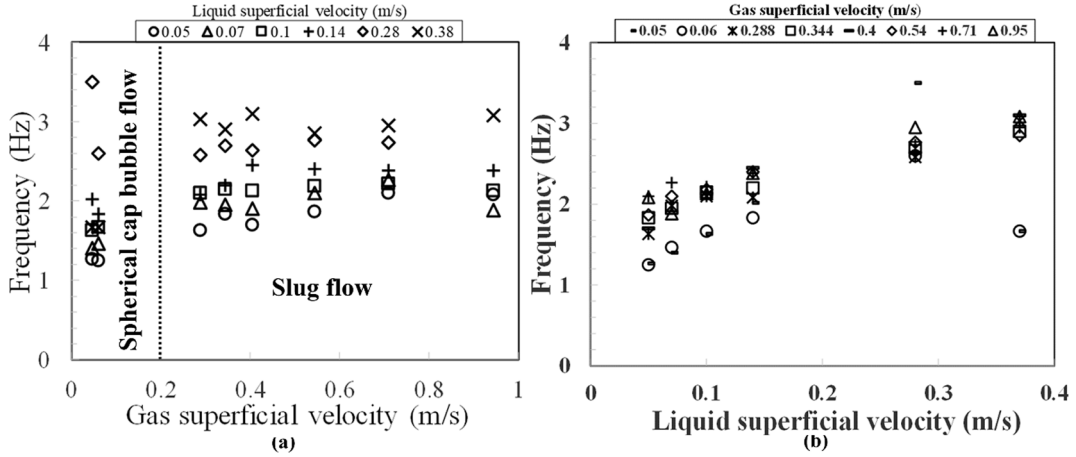

Fig. 9. Frequency against (a) gas superficial velocity for various liquid superficial velocities of 0.05–0.38 m/s and (b) liquid superficial velocity for gas superficial velocities of 0.05–0.95 m/s. Each of the experimental runs was repeated two times to check measurement repeatability. The average standard deviation of the data was ±2%.

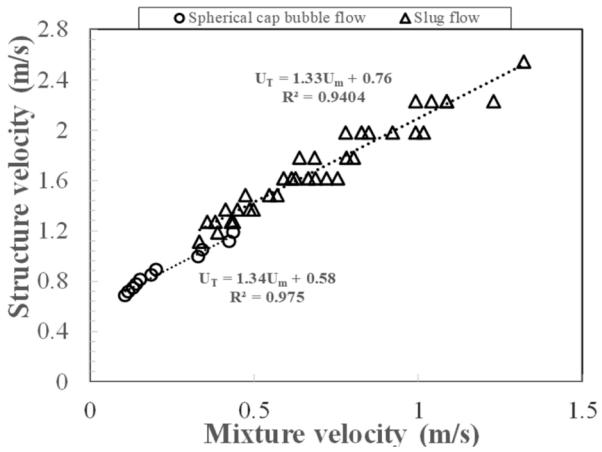

Fig. 11. Effect of mixture velocity on the bubbles structure velocity.

respectively. The structure velocity for the spherical cap bubble flow is lower than that of the slug flow. This interesting observation may be attributed to the existence of small bubbles in the slug unit, which may change the velocity profiles at slug tail or the Taylor bubble nose.

It is worth mentioning that the linear trend associated with the spherical cap bubble flow is not as apparent as that in the slug flow pattern. This could be due to the limited database available for the spherical cap bubble flow pattern in comparison to those for the slug flow regime.

A plot of structure velocity versus mixture velocity on a semi-logarithmic graph is shown in Fig. 12. The purpose is to emphasize the convergence of present data against the Nicklin et al. [58] correlations represented as equations (28) and (29), for turbulent and laminar flows, respectively.

$$U_T = 1.2U_M + 0.35\sqrt{gd} \tag{28}$$

$$U_T = 1.8U_M + 0.35\sqrt{gd} \tag{29}$$

The figure shows the existence of three distinct zones: in Zone 1 the structure velocity follows the equations (28) and (29); in Zone 2 there is a gradual deviation from these equations and in Zone 3 there is a far departure from them. These three zones can be associated with the various flow patterns, namely, spherical cap bubble, slug, and churn flows, respectively.

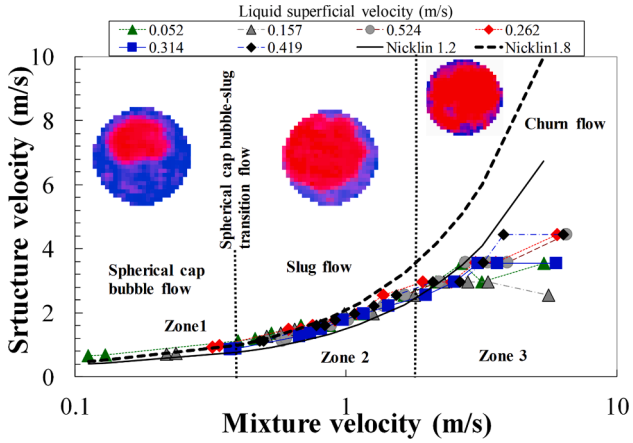

Fig. 12. A semi-logarithmic graph of bubbles structure velocity against the mixture velocity.

4.9. Time-averaged cross-sectional void fraction

The effect of gas superficial velocity on the time-averaged void fraction at liquid superficial velocities of 0.05–0.38 m/s is presented in Fig. 13. All the plots show similar tendency. At a constant liquid superficial velocity, the void fraction rises monotonically with the gas superficial velocity. Though, the average void fraction rises with a drop in the liquid superficial velocity. It is noteworthy that in the low-velocity limit, the void fraction grows swiftly with a rise in the gas superficial velocity. In contrast, in the high-velocity boundary, the void fraction develops gradually with the progressing gas superficial velocity.

Another interesting point observed in Fig. 13 is that the void fraction likewise varies with the flow pattern, with low void fraction values of $0.089 \leq \varepsilon \leq 0.23$ related to spherical cap bubble. This is consistent with the conclusions of Griffith and Synder [33]. With the rise of gas superficial velocity, the flow pattern swiftly becomes slug flow. The void fraction values are in the range of 0.27–0.62. This range for the slug flow regime agrees with the findings of Kendoush and Al-Khatab [50].

4.10. Reconstructed images shown by the WMS

Interrogation of the reconstructed images (virtual side views) accomplished from the series of cross-sectional frames provides vital in-depth knowledge of flow behaviour. As presented in Fig. 14a, at the lowest gas superficial velocity of 0.05 m/s, individual small bubbles, normally in clusters, can be seen appearing at the WMS. This is confirmed by visualisation using a high-speed camera. With the increase of gas superficial velocity to 0.40 m/s shown in Fig. 14b, large bubbles enveloping almost the entire pipe cross-section emerged. Notwithstanding, visualisation images show that these large bubbles do not have the typical feature of Taylor bubbles with bullet-shaped and smooth liquid films around them. In contrast, they are rounded with thicker and very wavy films. The bubbles are rounded, due to the significant effect of the surface tension of silicone at the liquid and gas superficial velocities of 0.05 and 0.4 m/s, respectively. As a result of the encountered high Reynolds number provoked by the somewhat high silicone oil viscosity, 0.005 kg/ms, there is a considerable enhancement of turbulence in the wake region of the Taylor bubble. Consequently, several vortices are observed, in the wake, hence, the interface, and thus the films remain very wavy and disturbed.

A similar observation made in Fig. 14b, is also seen here in Fig. 15a. The large Taylor bubbles do not have the traditional bullet-shape, including smooth films around them linked with the signature of

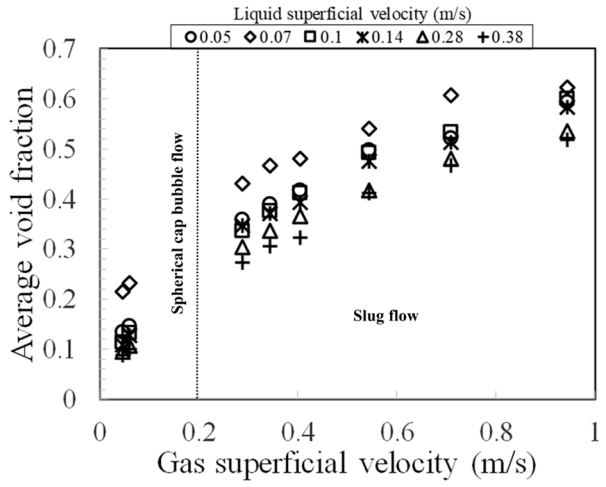

Fig. 13. The effect of gas superficial velocity on the time averaged void fraction at liquid superficial velocities of 0.05–0.38 m/s. Each of the experimental runs was repeated two times to check measurement repeatability. The average standard deviation of the data was ±2%.

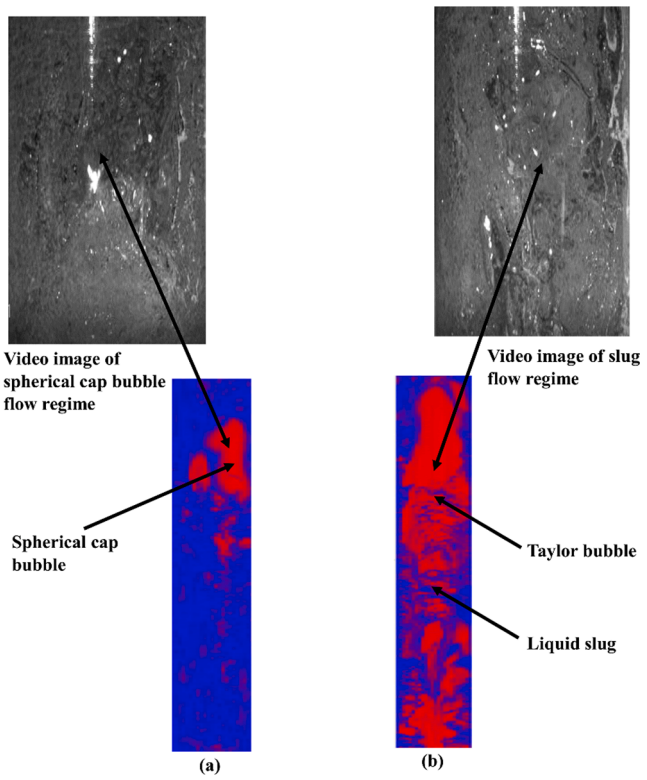

Fig. 14. Virtual lateral display of the transition from spherical cap bubble to slug flow validated by video images at the liquid superficial velocity of 0.05 m/s and gas superficial velocity (m/s) of (a) 0.05 and (b) 0.40.

Taylor bubbles, as shown in Fig. 15b and which are identified in small diameter pipes but have thicker, very wavy films around them.

4.11. *Present void fraction data versus the values from empirical correlations*

Fig. 16 presents a comparison between the results of present experimental values of void fraction against the values of void fraction obtained using the correlations by Nicklin et al. [58], Toshiba (2002), Bonnecaze et al. [18], and Dix [28]. For void fraction values less than 0.2, corresponding to the spherical cap bubble regime, the correlations by Nicklin et al. [58] (±1%) and Bonnecaze et al. [18] (±3%) offer better results than the Dix [28] (±7%). Unfortunately, the Dix [28] correlation under-predict void fraction values of between 0.2 and 0.23 also within the spherical cap bubble flow regime by about 12%. In contrast, for the values of void fraction > 0.3, representing slug flow regime, the correlation by Nicklin et al. [58] (±2%) provide superior

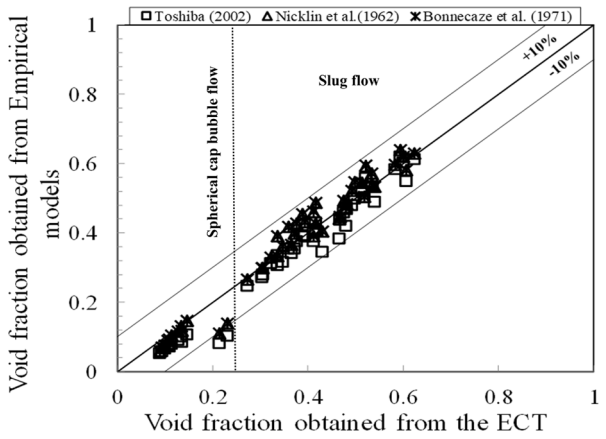

Fig. 16. Comparing the time averaged void fraction from the present experimental void fraction and the values obtained using the correlations by Nicklin et al. [58], Bonnecaze et al. [18], and Dix [28] Toshiba (2002).

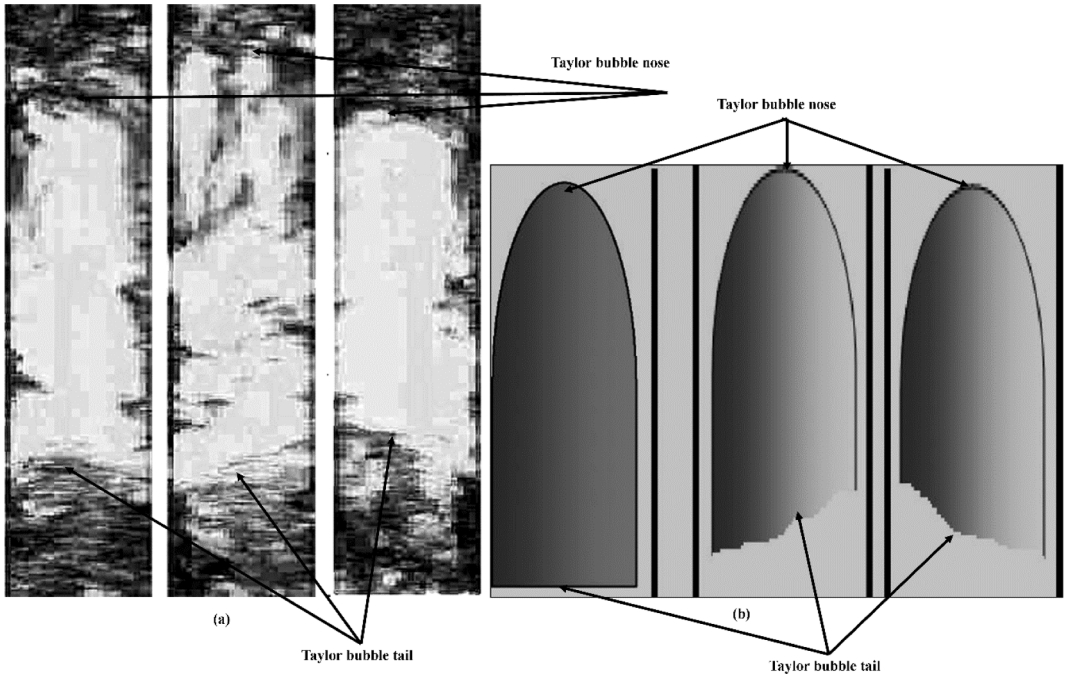

Fig. 15. Reconstructed images of slug flow from (a) present experimental work showing Taylor bubbles without the traditional bullet-shaped in a vertical 0.067 m diameter pipe and (b) traditional bullet-shaped Taylor bubbles as identified in small diameter pipes.

prediction than by Bonnecaze et al. [18] (±10%) and Dix [28] (±10%).

4.12. Experimental time-averaged radial void fractions

The effect of gas superficial velocity on the radial void fraction at the liquid superficial velocity of 0.05 m/s is shown in Fig. 17. The procedure for calculating the time-averaged radial void fraction involves spreading out (averaging) the localised instantaneous void fractions during the period of measurement and through several ring-formed regions. The details of how the time-averaged radial void fraction was calculated can be found in Abdulkadir et al. [7].

It can be observed from Fig. 17 that, at liquid and gas superficial velocities of 0.05 m/s and 0.05–0.7 m/s, respectively, two profiles are obtained, for the spherical cap bubble and slug flows. The profiles for the spherical cap bubble and slug flows are parabolic and semi-flat parabolic, respectively. The parabolic profiles show that the minimum and maximum radial void fractions are observed at the pipe wall (r/R = 1) and centre of the pipe (r/R = 0), respectively. The maximum range of radial void fraction values regarding the spherical cap bubble is $19.6 \leq \varepsilon \leq 22\%$ while, on the other hand, $50.8 \leq \varepsilon \leq 68.7\%$ for the slug flow. The profiles then proceeded downwards in a parabolic manner to a definite minimum. The minimum radial void fractions so obtained for the spherical cap bubble is $5.6 \leq \varepsilon \leq 6.2\%$ whereas $13.4 \leq \varepsilon \leq 19.6\%$ for slug flow. The transition from spherical cap bubble to slug flow based on the radial void fraction profiles can be attributed to the merging of smaller bubbles to form larger ones called Taylor bubbles. The results show that an increase in gas superficial velocity is responsible for the increase in the size of the bubbles including their density. The bubbles on reaching a point become so tightly bound that many impacts occur, and the rate of coalescing to create bigger bubbles increases unexpectedly, and the result is an increase in the radial void fraction at both the centre of the pipe and the pipe wall. It can be concluded from Fig. 17, therefore, that the shape of the radial void fraction profile, and an increase in percentage void fraction are dependent on the gas superficial velocity. The profiles obtained are in good agreement with the results obtained by Abdulkadir et al. [5].

4.13. Void fraction in the liquid slug, and Taylor bubble

4.13.1. Void fraction in the liquid slug:

Void fraction in the liquid slug is the fraction of the area occupied by the gas phase in the liquid slug to the area of the gas phase in the section containing gas and liquid. Fig. 18 shows that the void fraction in the liquid slug increases with a rise in the gas superficial velocity at a given liquid superficial velocity. The increase in the void fraction can be ascribed to the fact that an increase in the gas superficial velocity promotes the generation of bubbles and the growth of bubble size. Consequently, the void fraction in the liquid slug increases. It agrees with the findings of Abdulkadir et al. [4]. However, the liquid superficial velocity showed an insignificant effect on the void fraction in the liquid slug. It can be concluded based on Fig. 18 that the flow pattern is spherical cap bubble flow for $0.09 \leqslant \varepsilon_s \leqslant 0.19$, whilst for $0.18 \leqslant \varepsilon_s \leqslant 0.43$, the flow pattern is slug flow.

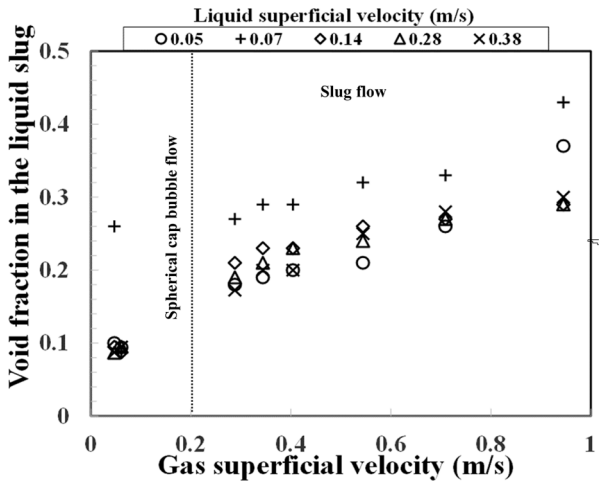

Fig. 18. The effect of the gas superficial velocity on the average void fraction in the liquid slug at liquid superficial velocities of 0.05–0.38 m/s. Each of the experimental runs was repeated two times to check measurement repeatability. The average standard deviation of the data was ±2%.

4.13.2. Void fraction in the Taylor bubble:

The void fraction in the Taylor bubble is the fraction of the area occupied by the gas phase in the Taylor bubble to the area of the gas phase in the section containing gas and liquid. Fig. 19 presents the effect of gas superficial velocity on the void fraction in the Taylor bubble. It is observed from the figure that the void fraction in the Taylor bubble increases as the gas velocity increases.

At a liquid and gas superficial velocities of 0.05 and 0.05–0.061 m/s, respectively, the void fraction in the Taylor bubble shown in Fig. 19 decreases from 0.23 to 0.2. As the gas superficial velocity is increased

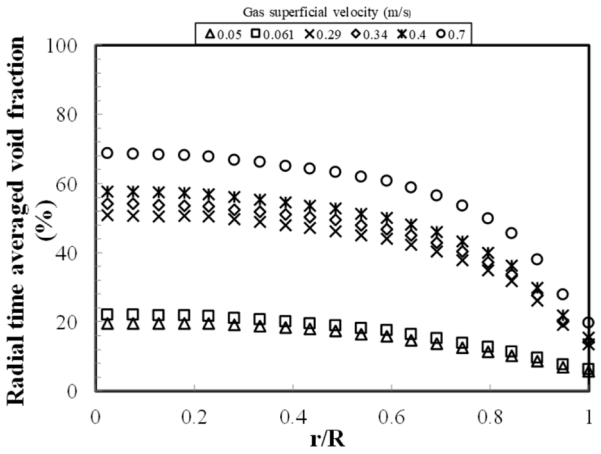

Fig. 17. The time-average radial void fraction distribution at liquid and gas superficial velocities of 0.05 and 0.05–0.7 m/s, respectively. r/R = 1 represents at the pipe wall whereas r/R = 0 represents at the centre of the pipe. Each of the experimental runs was repeated two times to check measurement repeatability. The average standard deviation of the data was.±5% ± 5%

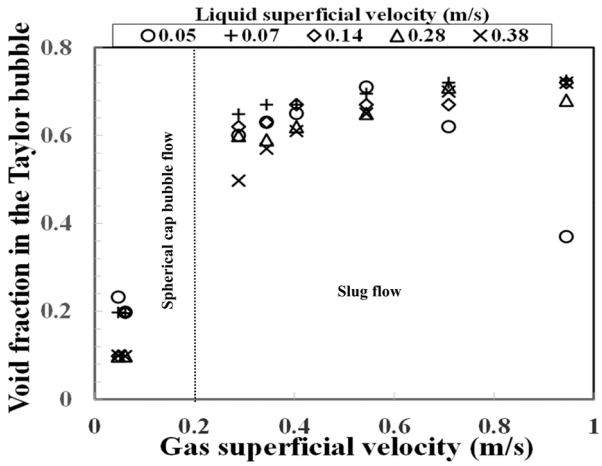

Fig. 19. The effect of the gas superficial velocity on the average void fraction in the Taylor bubble at the liquid superficial velocities of 0.05–0.38 m/s. Each of the experimental runs was repeated two times to check measurement repeatability. The average standard deviation of the data was ±2%.

from 0.29 to 0.95 m/s, the void fraction in the Taylor bubble increases until the terminal gas superficial velocity is reached at 0.54 m/s, it then drops to about 0.37. The increase in the gas superficial velocity provoked an increase in the numerous impacts between bubbles of various sizes happening, and the rate of coalescing to produce bigger bubbles grows suddenly. The result is consequently the transition from the spherical cap bubble to slug flow, and hence, a proposal that this phenomenon may be responsible for the increase in the void fraction in the Taylor bubble. The drop in the void fraction in the Taylor bubble, on the other hand, is perhaps described by a collapse of the Taylor bubble and is a transition to the spherical cap bubble from the slug flow regime.

Fig. 19 shows that when the liquid and gas superficial velocities are 0.07 and 0.38 m/s and 0.05–0.061 m/s, respectively, the void fraction in the Taylor bubble is independent of the gas superficial velocity. An exponential relationship is established between the void fraction in the Taylor bubble and the gas superficial velocity as the gas superficial velocity is increased from 0.29 to 0.40 m/s.

On the contrary, at a liquid and gas superficial velocities of 0.14 and 0.05–0.061 m/s, respectively, the void fraction in the Taylor bubble increases from about 0.1 to 0.2. With an increase in the gas superficial velocity from 0.29 to 0.40 m/s, the void fraction in the Taylor bubble increases from 0.62 to 0.67 and then remains constant before it finally increases to about 0.72 at a gas superficial velocity of 0.95 m/s. At a liquid and gas superficial velocities of 0.28 and 0.05–0.061 m/s, respectively, the void fraction in the Taylor bubble is independent of the gas superficial velocity. When the gas superficial velocity increases from 0.29 to 0.34 m/s, the void fraction in the Taylor bubble decreases a little and then increases from 0.59 to 0.71, and then it drops to about 0.68 at a gas superficial velocity of 0.95 m/s.

4.14. Lengths of liquid slug, Taylor bubble and slug unit

4.14.1. Length of the liquid slug:

Fig. 20 shows the effect of gas superficial velocity on the average liquid slug length. At liquid superficial velocities of 0.05–0.38 m/s and gas superficial velocities of 0.05–0.061 m/s, where the spherical cap bubble appears in both Fig. 20, is the growth of bubbles due to bubble coalescence. With an increase in gas superficial velocity to 0.29–0.95 m/s, where slug flow is present, it can be observed that there is no explicitly defined trend for the variation of the liquid slug length with gas superficial velocity owing to the continuous interaction between the bubbles in the liquid slug and the wake of the Taylor bubble.

However, it is interesting to note that at a liquid superficial velocity of 0.05 m/s, the liquid slug length can be seen to increase from approximately 2 to 9 pipe diameters and then decreases finally to around 5 pipe diameters. Also, the approximate shape of the best fit curve is a trapezium, with a pair of parallel sides. The average liquid slug length, according to Moissis and Griffith [57], for the case of a vertical pipe is in the range of 8–25 pipe diameters. A stable liquid slug length is reported to be between 10 and 20 pipe diameters [17] and [73] for an air–water system in a vertical pipe. The shorter liquid slug length obtained may be attributed to the bigger pipe diameter used in the present experiments. Based on reports, the slug flow pattern tends to disappear as the pipe diameter increases, Omebere-Iyari et al. [60]. Observed is a similar trend for a liquid superficial velocity of 0.38 m/s.

(a) Taylor bubble and slug unit lengths:

The effect of gas superficial velocity on the Taylor bubbles and slug unit lengths are depicted in Figs. 21 and 22, respectively. As expected, it is interesting to observe from the figures, that the Taylor bubble and slug unit lengths exhibit similar trends, revealing that the Taylor bubble is the principal contributor to the slug unit length.

At liquid superficial velocities of 0.05 and 0.1 m/s and gas superficial velocities of 0.05–0.061 m/s, where the spherical cap bubble appears in both Figs. 21 and 22, is the growth of bubbles owing to bubble coalescence. Maintaining the same gas superficial velocities but at liquid superficial velocities of 0.07, 0.28, and 0.38 m/s, where the spherical cap bubble also emerges, there are shortenings in both the Taylor bubble and slug unit lengths. As suggested by Hewitt [42], a growth in either the Taylor bubble or slug unit length implies that there is bubble coalescence, while a decrease signifies that there is a bubble breakup. Further increase in gas superficial velocity, where slug flow appears, the bubble density rises, supporting more impacts and coalescences and ultimately heading to the formation of longer bubbles.

4.15. Gravitational, frictional, and total pressure gradients

A differential pressure transducer (DP cell) was employed to measure the total pressure drop. The taps of the DP cell were placed around the twin-plane ECT, whereas the frictional pressure drop was determined by deducting the gravitational pressure drop term from the measured total pressure drop. The gravitational pressure drop, $(\Delta P)_{gr}$, was determined using equation (30)

$$(\Delta P)_{gr} = g\rho_H = g[\varepsilon\rho_G + (1-\varepsilon)\rho_L] \quad (30)$$

The gravitational pressure gradient was obtained by dividing the gravitational pressure drop with the separation distance between the

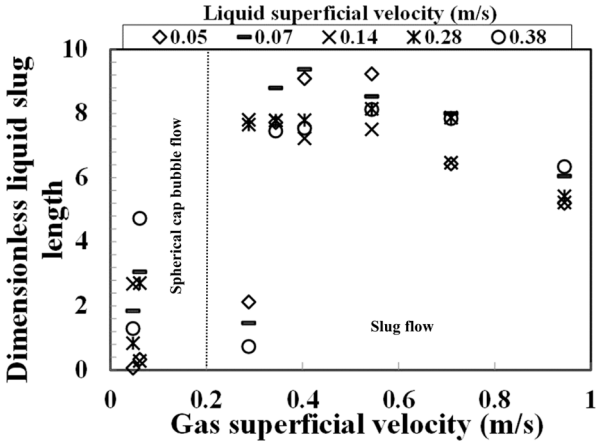

Fig. 20. The effect of the gas superficial velocity on the normalised average length of the liquid slug at liquid superficial velocities of 0.05–0.38 m/s. Each of the experimental runs was repeated two times to check measurement repeatability. The average standard deviation of the data was ±2%.

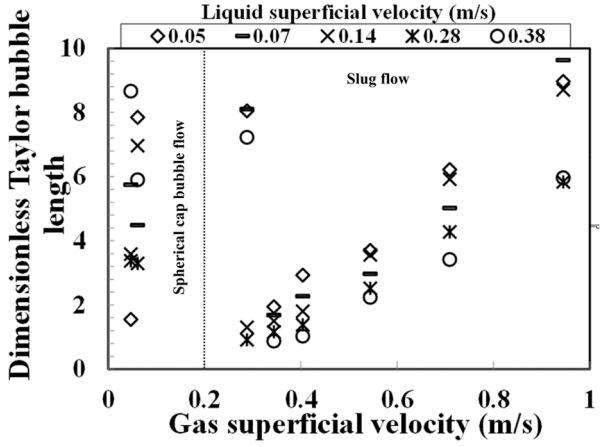

Fig. 21. The effect of the gas superficial velocity on the normalised average length of the Taylor bubble at liquid superficial velocities of 0.05–0.38 m/s. Each of the experimental runs was repeated two times to check measurement repeatability. The average standard deviation of the data was ±2%.

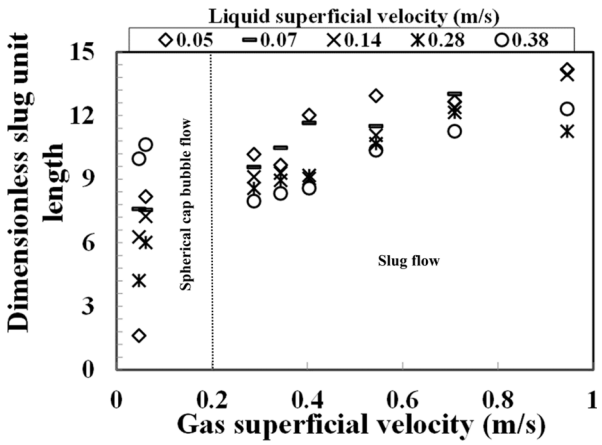

Fig. 22. The effect of the gas superficial velocity on the normalised average slug unit length at liquid superficial velocities of 0.05–0.38 m/s. Each of the experimental runs was repeated two times to check measurement repeatability. The average standard deviation of the data was ±2%.

two tappings. The distance of separation between the two DP cell tappings is 0.86 m. A similar procedure was employed to determine the frictional and total pressure gradients.

Shown in Fig. 23(a–c) is the effect of gas superficial velocity on the gravitational, frictional, and total pressure gradients. Fig. 23a depicts a decrease in the gravitational pressure gradient because of an increase in the gas superficial velocity. The decrease in the gravitational pressure gradient can be explained by the fact that an increase in gas superficial velocity provokes an increase in the void fraction, thereby reducing the mixture density because of a decrease in the liquid hold up. It is worth mentioning that at low gas superficial velocities of 0.05–0.1 m/s, the gravitational pressure gradients encountered in the spherical cap bubble flow regime are higher than those witnessed in the slug flow regime. This is not surprising because the void fractions in the spherical cap bubble flow in comparison to the slug flow regime are smaller with attendant higher liquid holdups. This results in the observed higher gravitational pressure gradient in the spherical cap bubble regime.

Fig. 23b, on the contrary, shows that the frictional pressure gradient increases with an increase in the gas superficial velocity. This behavior may be attributed to the increasing drag encountered by the bubbles and the coalescence of the gas bubbles. These observations support the phenomena recently reported by Abdulkadir et al. [4], who worked on a vertical 67 mm internal diameter pipe using air–silicone oil as the working fluid. It is worthy of mention that at gas superficial velocities of 0.05–0.1 m/s, wherein the size of the bubbles in the slug flow regime are expected to be bigger than those in the spherical cap bubbles, the frictional pressure gradients encountered in the slug flow regime are higher than those in the spherical cap bubble flow regime.

The total pressure gradient displayed in Fig. 23c also decreases with an increase in the gas superficial velocity. The observed decrease in the total pressure gradient can be described by the fact that the flow in the vertical pipe is gravity dominated, i.e., the main contributor to the total pressure gradient is the gravitational pressure gradient. Consequently, the total pressure gradient also decreases with an increase in the gas superficial velocity. A similar observation seen in Fig. 23a at low gas superficial velocities of 0.05–0.1 m/s is also observed here in Fig. 23c, the total pressure gradients encountered in the spherical cap bubble flow regime are higher than those witnessed in the slug flow regime. This is not surprising because the void fractions in the spherical cap bubble flow in comparison to the slug flow regime are smaller with attendant higher liquid holdups. This results in the observed higher total pressure gradient in the spherical cap bubble regime.

4.16. Comparison of experimental data with the values from published transition boundary models

In this work, the model proposed in Taitel et al. [71] was modified to define the transition boundary, as displayed in Fig. 24, whereby the measured average cross-sectional void fraction is used instead of the

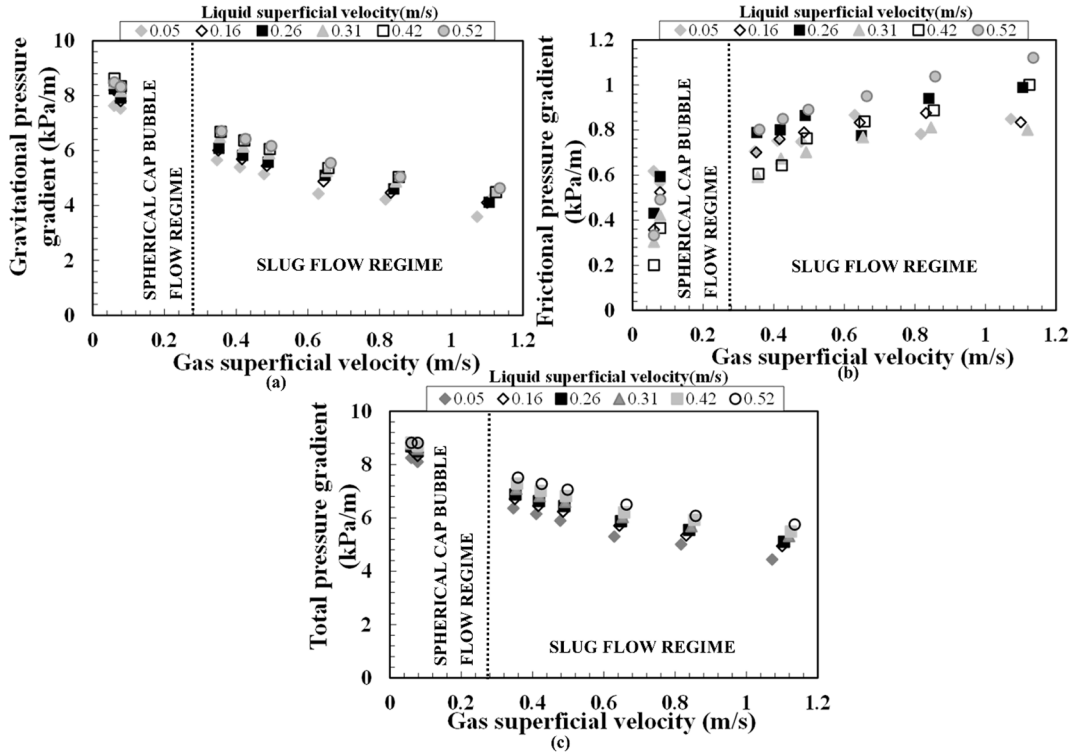

Fig. 23. The influence of the gas superficial velocity on the (a) gravitational (b) frictional (c) total pressure gradients at liquid and gas superficial velocities of 0.05–0.52 m/s and 0.05–1.15 m/s, respectively.

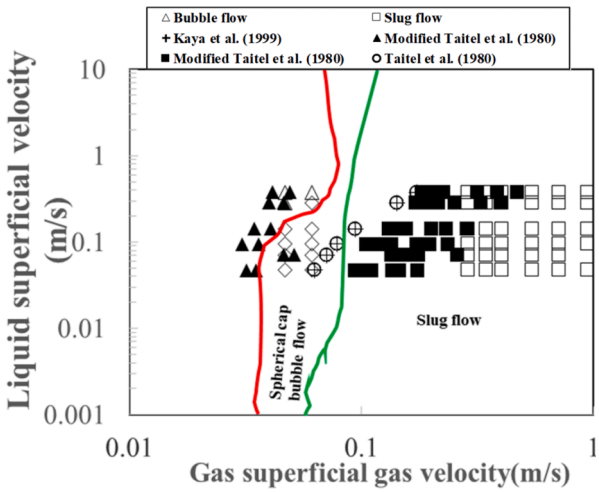

Fig. 24. Flow pattern map showing present experimental data including comparison against other models.

hitherto fixed critical cross-sectional void fraction of 0.25. From the figure, the red line symbolises the shift from bubble to spherical cap bubble flow, while the green line indicates the transition to slug flow from spherical cap bubble. It is worthy of mention, according to the figure, that the obtained result signifies better accord with the present experimental data than those by the Taitel et al. [71] and Kaya et al. [48] models.

Established from Fig. 24 are three flow regimes, namely, bubble, spherical cap bubble, and slug flow regimes. The spherical cap bubble transition happens at the void fraction of 0.13 while, on the other hand, slug flow takes occurs at the void fraction of 0.3. Furthermore, based on experimental data, the transitional gas superficial velocity at which the spherical cap bubble flow appears steadily is between 0.04 and 0.06 m/s, which is just to the left of the green transition line. The ensuing flow regime at low gas superficial velocities is bubble flow, whereas, at higher gas superficial velocities, slug flow is apparent. In between, at the relatively low gas superficial velocities, spherical cap bubble flow prevails, that is marked by long deformed bubbles nearly enveloping the entire pipe cross-section but moving at intervals with smaller diameter bubbles flowing behind them.

5. Conclusion

An ECT, WMS, and DP cell were utilized in this work to carry out detailed experimental investigation on the characteristics of the transition from the spherical cap bubble to slug flow in a vertical 6 m in height and an internal diameter of 0.067 m pipe. The system fluids used were air and silicone oil. The experimental data campaign was carried out for a series of liquid and gas superficial velocities of 0.05 to 0.52 m/s and 0.05 to 4.7 m/s, respectively. Data acquisition frequencies for the ECT, WMS, and DP cell are 200, 1000, and 1000 Hz, respectively. The summary of the key findings is:

1. The major flow patterns observed in the present study are spherical cap bubble and slug flows and were found to be consistent with those reported in the literature. ECT and WMS give a reasonably good agreement within ±10%on void fraction measurements.
2. A rise in gas superficial velocity provokes a flow pattern transition to slug flow from the spherical cap bubble. Although, there was no information reported in this work about the perturbation that is well known to be responsible for the abrupt change, the spherical cap bubble at the liquid superficial velocity of 0.38 m/s changes abruptly into the bubble flow.

Also, the shrinkage of the widening tail of the spherical cap bubble and a collapse in the size of the Taylor bubbles can be attributed to the superiority of the high liquid velocity (the flow regime is turbulent flow based on the liquid phase Reynolds number) which subdued the surface tension forces that keeps the large bubbles together. Consequently, the bubbles are broken down into smaller ones, leading to the formation of bubbly flow regime.

3. The condition at which the plot of structure velocity against mixture velocity began to deviate from the Nicklin et al. [58]'s curves coincides with the transition boundaries from spherical cap bubble to slug flows and to churn flow from slug flow.
4. The void fraction rises swiftly with increasing gas superficial velocity in the low-velocity limit and develops gradually with an increase in the gas superficial velocity in the high-velocity limit. The match between current experimental data with the values from the empirical correlations of Nicklin et al. [58], Bonnecaze et al. [18], and Dix [28] Toshiba (2002) shows that the correlation of Nicklin et al. [58] provides superior prediction for both the spherical cap bubble and slug flows.
5. The gravitational and total pressure gradients along the pipe were observed to decrease as the gas superficial velocity increases, whereas the measured frictional pressure gradient was found to increase.
6. The flow patterns established for the void fraction in the liquid slug is spherical cap bubble flow for $0.09 \leqslant \varepsilon_s \leqslant 0.19$and slug flow for $0.18 \leqslant \varepsilon_s \leqslant 0.43$. The flow patterns based on the slug unit length is $4 \leqslant L_u/D \leqslant 11$for spherical cap bubble flow and $8 \leqslant L_u/D \leqslant 16$ for slug flow.
7. Found was a reasonably good agreement for comparison between the amended Taitel et al. [71] and the modified Kaya et al. [48] transition boundary models with the current experimental data.
8. A plot of PSD against frequency helped in showing how the flow pattern changes by its shape with liquid and gas superficial velocities. The frequency obtained from the PSD were seen to increase with increasing liquid superficial velocity. The number of main peaks (regarded as harmonics) for the spherical cap bubble flow intensifies with a rise in the liquid superficial velocity.
9. The plot of Strouhal number against input liquid content showed that the interdependence between frequency and liquid superficial velocity is nearly linear; signifying that correctly predicted is the influence of liquid superficial velocity using velocity and length scales.

This study has provided a more fundamental insight into the physical phenomena that govern the behaviour of the transition from spherical cap bubble to slug flow regime and the way these parameters behave under various flow conditions.

6. Author statement

I attach a revised manuscript entitled ""Experimental investigation of the characteristics of the transition from spherical cap bubble to slug flow in a vertical pipe" for consideration for publication in the Experimental Thermal and Fluid Science. This is a declaration that our manuscript has not been published or submitted elsewhere and that all cited materials have been duly acknowledged.

Declaration of Competing Interest

I attach a revised manuscript entitled "Experimental investigation of the characteristics of the transition from spherical cap bubble to slug flow in a vertical pipe" for consideration for publication in the Experimental Thermal and Fluid Science. All bodies that have anything to this work were duly acknowledged. This is also to let you know that there is no conflict of interest.

Acknowledgement

Abdulkadir, M., would like to express his sincere appreciation to the Nigerian government through the Petroleum Technology Development Fund (PTDF) for providing the funding for his doctoral studies.

This work has been undertaken within the Joint Project on Transient Multiphase Flows and Flow Assurance. The Author(s) wish to acknowledge the contributions made to this project by the UK Engineering and Physical Sciences Research Council (EPSRC) and the following: - GL Industrial Services; BP Exploration; CD-adapco; Chevron; ConocoPhillips; ENI; ExxonMobil; FEESA; IFP; Institutt for Energiteknikk; PDVSA (INTEVEP); Petrobras; PETRONAS; SPT; Shell; SINTEF; Statoil and TOTAL. The Author(s) wish to express their sincere gratitude for this support.

References

[1] M. Abdulkadir, Experimental and computational fluid dynamics (CFD) studies of gas–liquid flow in bends, PhD Thesis, University of Nottingham, UK, 2011.
[2] M. Abdulkadir, A. Abolore, C.N. Eastwick, B.J. Azzopardi, I.E. Smith, T.E. Unander, Investigating the effect of pressure on a vertical two-phase upward flow with a high viscosity liquid, AIChE J. 66 (2020) 1–16.
[3] M. Abdulkadir, V. Hernandez-Perez, C.A. Kwatia, B.J. Azzopardi, Interrogating flow development and phase distribution in vertical and horizontal pipes using advanced instrumentation, Chem. Eng. Sci. 186 (2018) 152–167.
[4] M. Abdulkadir, V. Hernandez-Perez, I.S. Lowndes, B.J. Azzopardi, S. Dzomeku, Experimental study of the hydrodynamic behaviour of slug flow in a vertical riser, Chem. Eng. Sci. 106 (2014) 60–75.
[5] M. Abdulkadir, V. Hernandez-Perez, I.S. Lowndes, B.J. Azzopardi, E.T. Brantson, Detailed analysis of phase distributions in a vertical riser using wire mesh sensor (WMS), Exp. Therm Fluid Sci. 59 (2014) 32–42.
[6] M. Abdulkadir, V. Hernandez-Perez, I.S. Lowndes, B.J. Azzopardi, E. Sam-Mbomah, Experimental study of the hydrodynamic behaviour of slug flow in a horizontal pipe, Chem. Eng. Sci. 156 (2016) 147–161.
[7] M. Abdulkadir, V. Hernandez-Perez, I.S. Lowndes, B.J. Azzopardi, S. Sharaf, Experimental investigation of phase distributions of two-phase air–silicone oil flow in a vertical pipe, World Academy Science Eng. Technology 4 (2010) 18–25.
[8] M. Abdulkadir, D.G. Jatto, L.A. Abdulkareem, D. Zhao, Pressure drop, void fraction and flow pattern of vertical air–silicone flows using differential pressure transducer and advanced instrumentation, Chem. Eng. Res. Des. 159 (2020) 262–277.
[9] M. Abdulkadir, D. Zhao, S. Sharaf, L.A. Abdulkareem, I.S. Lowndes, B.J. Azzopardi, Interrogating the effect of 90° bends on air–silicone oil flows using advanced instrumentation, Chem. Eng. Sci. 66 (2011) 2453–2467.
[10] L. Abdulkareem, Tomographic investigation of gas–oil flow in inclined risers, PhD Thesis, University of Nottingham, UK, 2011.
[11] L. Abdulkareem, B.J. Azzopardi, S. Thiele, A. Hunt, M.J. Da Silva, Interrogation of gas/oil flow in a vertical pipe using tomographic techniques, Offshore Geotechnics Petroleum Technology 7 (2009).
[12] A. Abdullahi, M. Abdulkadir, V. Hernandez-Perez, L.A. Abdulkareem, S. Sharaf, B. J. Azzopardi, Investigating the effect of pipe inclination on two-phase gas-liquid flow using advanced instrumentation, ASME/JSME 8th Thermal Joint Conference (2011).
[13] Azzopardi, B. J., Abdulkareem, L. A., Zhao, D., Thiele, S., Da Silva., M. J., Beyer, M., and Hunt, A., 2010. Comparison between electrical capacitance tomography and wire mesh sensor output for air/silicone oil flow in a vertical pipe. Industrial Engineering Chemical Research 49.
[14] B.J. Azzopardi, I. Amadi, S. Yang, L.A. Abdulkareem, A. Azzi, M. Abdulkadir, Persistence of frequency in gas–liquid flows across a change in pipe diameter or orientation, Int. J. Multiph. Flow 67 (2014) 22–31.
[15] Azzopardi, B. J., 2006. Gas–liquid flows, Begell house.
[16] G.K. Bachelor, An introduction to fluid dynamics, Cambridge University Press, 1967.
[17] D. Barnea, L. Shemer, Void fraction measurements in vertical slug flow: applications to slug characteristics and transition, Int. J. Multiph. Flow 15 (1989) 495–504.
[18] K.H. Bonnecaze, W. Erskine, E.J. Greskovich, Holdup and pressure drop for two-phase slug flow in inclined pipelines, *AIChE* J. 17 (1971) 1109–1113.
[19] J.M. Boulton-Stone, P.B. Robinson, J.R. Blake, A note on the axisymmetric interaction of pairs of rising, deforming gas bubbles, Int. J. Multiph. Flow 21 (1995) 1237–1241.
[20] W. Bousman, J. Mcquillen, L. Witte, Gas–liquid flow patterns in microgravity: effects of tube diameter, liquid viscosity, and surface tension, Int. J. Multiph. Flow 22 (1996) 1035–1053.
[21] J.P. Brill, H. Mukherjee, Multiphase Flow in Wells Monograph Series, SPE, Richardson, Texas, 1999.
[22] R. Collins, F.F. De Moraes, J.F. Davidson, D. Harrison, The motion of a large gas bubble rising through liquid flowing in a tube, J. Fluid Mech. 89 (1978) 497–514.
[23] G. Costigan, P.B. Whalley, Slug flow regime identification from dynamic void fraction measurements in vertical air–water flows, Int. J. Multiph. Flow 23 (1997) 263–282.
[24] R.K. Das, S. Pattanayak, Bubble to slug flow transition in vertical upward two-phase flow through narrow tubes, Chem. Eng. Sci. 49 (1994) 2163–2172.
[25] M.J. da Silva, Impedance sensors for fast multiphase flow measurement and imaging, PhD Thesis, Technische Universität Dresden, 2008.
[26] M.J. da Silva, E. Schleicher, U. Hampel, Capacitance wire-mesh sensor for fast measurement of phase fraction distributions, Measurement Science Technology 18 (2007) 2245–2251.
[27] R.M. Davies, G.I. Taylor, The mechanics of large bubbles rising through extended liquids and through liquids in tubes, Proc. Royal Society, A 200 (1950) 375–395.
[28] G.E. Dix, Vapour void fractions for forced convection with sub cooled boiling at low flow rates, Ph.D. thesis, University of California, Berkeley, 1971.
[29] A.E. Dukler, J. Fabre, Gas–liquid slug flow, Multiphase Sci. Technology 8 (1994) 355–469.
[30] D.T. Dumitrescu, Stromung an einer luftblase in senkrechten rohr Z angrew Math Mech 23 (1943) 139–149.
[31] F.M. Exner, Physics Z. 28 (1927) 825–829.
[32] G.W. Govier, B.A. Radford, J.S.C. Dunn, The upward vertical flow of air-water mixtures, The Canadian Journal of Chemical Engineering 35 (1957) 58–70.
[33] Griffith, P. and Synder, G. A., 1964.The bubble-slug transition in a high velocity two phase flow MIT Report 5003-29 (TID-20947).
[34] P. Griffith, G.B. Wallis, Two-phase slug flow, J. Heat Transfer 83 (1961) 307–320.
[35] S. Guet, G. Ooms, R.V.A. Oliemans, Influence of bubble size on the transition from low-Re bubbly flow to slug flow in a vertical pipe, Exp. Therm Fluid Sci. 26 (2002) 635–641.
[36] S. Guet, G. Ooms, R.V.A. Oliemans, R.F. Mudde, Bubble size effect on low liquid input drift-flux parameters, Chem. Eng. Sci. 59 (2004) 3315–3329.
[37] L.S. Hansen, S. Pederson, P. Durdevic, Multiphase flow metering in offshore oil and gas transportation pipelines: trends and perspectives, Sensors 19 (2019) 1–26.
[38] J.F. Harper, The motion of bubble and drops through liquids, Advanced Applied Mechanics 12 (1972) 59–129.
[39] N.M. Hasan, B.J. Azzopardi, Imaging stratifying liquid–liquid flow by capacitance tomography, Flow Meas. Instrum. 18 (241) (2007) 246.
[40] V. Hernandez-Perez, Gas–liquid two-phase flow in inclined pipes, PhD thesis, University of Nottingham, 2008.
[41] V. Hernandez Perez, B.J. Azzopardi, R. Kaji, M.J. da Silva, M. Beyer, U. Hampel, Wisp-like structures in vertical gas-liquid pipe flow revealed by Wire Mesh Sensor studies, Int. J. Multiph. Flow 36 (2010) 908–915.
[42] Hewitt G. F., 1990. Non-equilibrium two-phase flow. Proceedings of the 9th International Heat Transfer Conference, Jerusalem 1, 383-394.
[43] J.H. Hills, The rise of a large bubble through a swarm of smaller ones, Transaction of Institution of Chemical Engineers 53 (1975) 224–233.
[44] J.H. Hills, R.C. Darton, Rising velocity of large bubbles in a bubble swarm, Transaction of Institution of Chemical Engineers 54 (1976) 258–264.
[45] Z. Huang, B. Wang, H. Li, Application of electrical capacitance tomography to the void fraction measurement of two-phase flow, IEEE Trans. Instrum. Meas. 52 (2003) 7–12.
[46] W.P. Jepson, R.E. Taylor, Slug flow and its transition in large diameter horizontal pipes, Int. J. Multiph. Flow 19 (1993) 411–420.
[47] D.D. Joseph, Rise velocity of a spherical cap bubble, J. Fluid Mech. 488 (2003) 213–223.
[48] Kaya, A. S., Sarica, C. and Brill, J. P., 1999. Comprehensive mechanistic modelling of two-phase flow in deviated wells. paper SPE 56522 presented at 1999 SPE Annual Technical Conference and Exhibition Houston, Texas, October.
[49] V.C. Kelessidis, A.E. Dukler, Modelling flow pattern transitions for upward gas–liquid flow in vertical concentric and eccentric annuli, Int. J. Multiph. Flow 15 (1989) 173–191.
[50] Kendoush, A.A. and Al-Khatab, S.A.W., 1989. Flow regimes characterization in vertical downward two phase flow. In: Chen, X.Z., Veziroglu, T.N., Tien, C.L. (Eds.), Multiphase Flow and Heat Transfer, Second International Symposium I, 215-220.
[51] K.W. Lawrence, P.C. Jiaping, H. Yung-Tse, K.S. Nazih, Membrane and desalination technologies, Springer Science and Business Media, 2010.
[52] S. Li, Y. Ma, S. Jiang, T. Fu, The drag coefficient and the shape of a single bubble rising in non-Newtonian fluids, J. Fluids Eng. 134 (2012) 669–679.
[53] Marashdeh, Q., 2009. Validation of electrical capacitance volume tomography with applications to multiphase flow system. MSc Thesis, The Ohio State University, Columbus, OH.
[54] A. Matuszkiewicz, J.C. Flamand, J.A. Boure, The bubble-slug flow pattern transition and instabilities of void fraction waves, Int. J. Multiph. Flow 13 (1987) 199–217.
[55] K. Mishima, I. Ishii, Flow regime transition criteria for two phase flow in vertical tubes, Int. J. Heat Mass Transf. 27 (1984) 723–734.
[56] S.K. Mohammed, A.H. Hassan, A. Ibrahim, G. Dimitrakis, B.J. Azzopardi, Dynamics of flow transitions from bubbly to churn flow in high viscosity oils and large diameter columns, Int. J. Multiph. Flow 120 (2019), 103095.
[57] R. Moissis, P. Griffith, Entrance effects in two-phase slug flow, ASME Journal of Heat Transfer (1962) 366–370.
[58] D.J. Nicklin, J.O. Wilkes, J.F. Davidson, Two-phase flow in vertical tubes, Transaction of Institution of Chemical Engineers 40 (1962) 61–68.
[59] N.K. Omebere-Iyari, B.J. Azzopardi, A study of flow patterns for gas/ liquid flow in small diameter tubes, Chem. Eng. Res. Des. 85 (2007) 180–192.
[60] N.K. Omebere-Iyari, B.J. Azzopardi, D. Lucas, M. Beyer, H.M. Prasser, The characteristics of gas–liquid flow in large diameter risers at high pressures, Int. J. Multiph. Flow 34 (2008) 461–476.
[61] J.-Y. Parlange, J. Fluid Mech. 37 (1969) 257–263.

[62] E. Pereyra, C. Torres, FLOPATN—Flow Pattern Prediction and Plotting Computer Code, The University of Tulsa, Tulsa, OK, 2005.
[63] C. Pradeep, R. Yan, S. Vestol, M.C. Melaaen, S. Mvylvaganam, Electrical capacitance tomography (ECT) with gamma radiation meter for comparison with and validation and tuning of computational fluid dynamics (CFD) modelling of multiphase flow, Meas. Sci. Technol. 25 (2014) 075404.
[64] H.-M. Prasser, R. Hafeli, Signal response of wire-mesh sensors to an idealized bubbly flow, Nucl. Eng. Des. 336 (2018) 3–4.
[65] Radovcich, N. A. and Moisis, R., 1962. The transition from two phase bubble flow to slug flow. MIT Report 7-7673-22.
[66] H. Shaban, S. Tavoularis, The accuracy of gas flow rate measurements in gas–liquid flows by cross-correlating dual wire-mesh sensor signals, Int. J. Multiph. Flow 78 (2016) 70–74.
[67] O. Shoham, Mechanistic modelling of gas–liquid two-phase flow in pipes, Society of Petroleum Engineers, USA, 2005.
[68] W. Siemes, Chemical Ing.-Tech 26 (1954) 614–630.
[69] C.H. Song, H.C. No, M.K. Chung, Investigation of bubble flow developments and its transition based on the instability of void fraction waves, Int. J. Multiph. Flow 21 (1995) 381–404.
[70] J.Y. Sun, W.P. Jepson, Slug flow characteristics and their effect on corrosion rates in horizontal oil and gas pipelines, paper SPE 24787 presented at the 67th Annual Technical Conference and Exhibition of the Society of Petroleum Engineers (1992).
[71] Y. Taitel, D. Barnea, A.E. Dukler, Modelling flow pattern transitions for steady upward gas–liquid flow in vertical tubes, *AIChE* J. 26 (1980) 345–354.
[72] C. Tompkins, H.-M. Prasser, M. Corradini, Wire-mesh sensors: A review of methods and uncertainty in multiphase flows relative to other measuring techniques, Nucl. Eng. Des. 337 (2018) 205–220.
[73] R. van Houst, L. Shemer, D. Barnea, Evolution of hydrodynamic and statistical parameters of gas-liquid slug flow along inclined pipes, Chem. Eng. Sci. 58 (2003) 115–133.
[74] F. Viana, R. Pardon, R. Yanez, J.L. Trallero, D.D. Joseph, Universal correlation for the rise velocity of long bubbles in round pipes, J. Fluid Mech. 494 (2003) 379–398.
[75] P. Venkateswararao, R. Semiat, A.E. Dukler, Flow pattern transitions for gas–liquid flows in vertical rod bundle, Int. J. Multiph. Flow 8 (1982) 509–524.
[76] Vuong, D.H., aydin, T.B., Torres, C.F., Schleicher, E., Pereyra, E., and Sarica, 2015. A methodology to quantify the uncertainty in liquid holdup measurements with wire-mesh sensor. Flow Measurement and Instrumentation 46, 18–24.
[77] G.R. Wallis, One-dimensional two-phase flow, McGraw-Hill, New York, 1969.
[78] G. Wang, M. Zhang, M. Ishii, Flow structure of bubbly to slug transition flow in small pipe, Int. J. Heat Mass Transf. 147 (2020) 1–13.
[79] E.T. White, R.H. Beardmore, The velocity of rise of single cylindrical air bubbles through liquids contained in vertical tubes, Chem. Eng. Sci. 17 (1962) 351–361.
[80] P.M. Wilkinson, A. Van Schayk, J.P.M. Spronken, L. Van Dierendonck, The influence of gas density and liquid properties on bubble breakup, Chem. Eng. Sci. 48 (1993) 1213–1226.
[81] Zhao, D., Omar, R., Abdulkadir, M., Azzi, A., Saidj, F., Hernandez-Perez, V., Hewakandamby, B. N., and Azzopardi, B. J., 2017. The control and maintenance of desired flow patterns in bends of different orientations". Flow Measurement and Instrumentation, 53, Part B, 230-242.
[82] M. Zhang, L.-M. Pan, P. Ju, X. Yang, M. Ishii, The mechanism of bubbly to slug flow regime transition in air–water two phase flow: A new transition criterion, Int. J. Heat Mass Transf. 108 (2017) 1579–1590.
[83] J. Bendat, A. Piersol, Engineering Application of Correlation and Spectral Analysis, John Wiley and Sons, New York, USA, 1980.